WIND TUNNEL TESTS ON A LOW-WING MONOPLANE WITH PROPELLER RUNNING

BY

SHIRLEY S. MILLER

AND

WALTER H. ALBACH

Thesis
M59

WIND TUNNEL TESTS ON A LOW-WING MONOPLANE WITH PROPELLER RUNNING

Thesis by

S. S. Miller and W. H. Albach
LIEUTENANTS, U.S. NAVY

In partial fulfillment of the requirements for

the Degree of Master of Science in Aeronautical Engineering

California Institute of Technology

Pasadena, California

1937

List of Figures

Table of Notations

a = slipstream factor, explained in text

$a_o = \frac{dC_L}{d\alpha_o}$ = slope of lift curve for infinite aspect ratio

A = area of propeller disc

AR = aspect ratio of wing

AR_t = aspect ratio of tail surfaces

B = a factor explained in text

b = wing span

β = propeller blade angle setting, at 75% radius

C_H = hinge moment coefficient

C_{H_o} = a factor explained in text

C_R = resultant drag coefficient = $\frac{D - T}{qS}$

C.G. = center of gravity of airplane

C_L = lift coefficient = L/qS

C_M = pitching moment coefficient = $M/qS\ell$

C_{M_o} = moment coefficient of wing about mean aerodynamic center

C_{M_W} = pitching moment coefficient of wing alone

$C_{M_{W+F}}$ = pitching moment coefficient of wing and fuselage = C_M(no tail)

C_{M_t} = pitching moment coefficient of tail

$C_{M_{th}}$ = pitching moment coefficient due to thrust

C_{M_F} = pitching moment coefficient of fuselage

C_y = yawing moment coefficient = $\frac{\text{Yawing moment}}{qbS}$

d = distance from leading edge of wing to C.G.

D = drag, a force parallel to air velocity

D_F = fuselage diameter

D_P = propeller diameter

e = elevator angle

e_t = elevator tab angle

H.M. = hinge moment

J = advance ratio = V/nD_p

k = a constant

K = a factor explained in text

L = lift, a force normal to air velocity

ℓ = tail length (C.G. to elevator hinge)

M = pitching moment of model about C.G.

n = revolutions per second

P = power

q = dynamic pressure = $\frac{1}{2}\rho V^2$

Q = torque

Q_c = torque coefficient

r = rudder angle

$\overline{r}$ = propeller radius = $D_p/2$

R = a factor explained in text

$\overline{R}$ = a factor explained in text

s = angle of incidence of stabilizer

S = wing area

S_t = tail area (horizontal surfaces)

T = thrust

T_c = thrust coefficient

t = mean aerodynamic chord length

t_e = SEE FIGURE 6.2

V = air velocity

W = weight of the airplane

α = angle of attack

α_u = geometrical angle of attack

α_s = geometrical angle of attack of horizontal stabilizer

α_d = aerodynamic decalage

Δ = "increment of"

η_t = tail efficiency

θ = angle of climb or glide

ρ = air density

σ = an angle, explained in text

ψ = angle of yaw

$(\ )'$ = $(\ )$ "power on"; e.g. $C_H' = C_H$ "power on", etc.

h = distance from leading edge of wing to mean aerodynamic center

ΔC_{M_o} = increment of moment coefficient change at $C_L = 0$ due to fuselage

ΔC_{M_t} = a factor explained in text

ΔF = a factor explained in text

List of References

1. Russell and McCoy, Journal of the Aeronautical Sciences, Vol. 3, No. 3, January 1936.

2. Malina and Jenney, Journal of the Aeronautical Sciences, Vol. 3, No. 7, May 1936.

3. C. B. Millikan and A. L. Klein: "Description and Calibration of 10 ft. Wind Tunnel at California Institute of Technology", presented at Berkeley meeting of the Aeronautics Division A.S.M.E., June 1932.

4. Thesis by Lt.-Comdr. C. M. Bolster, U.S.N., at California Institute of Technology, 1936.

WIND TUNNEL TESTS ON A LOW-WING MONOPLANE WITH PROPELLER RUNNING

Introduction

Various tests have been conducted on airplane wind tunnel models with an operating propeller in an endeavor to furnish the industry data as an aid in design and performance predictions. At the GALCIT, these investigations have comprised the material set forth in references 1, 2 and 4 .

The tests conducted by the authors of this paper represent a continuation of the above-mentioned investigations. The purpose of the present tests was to determine 1) the effect of power on static longitudinal stability (elevator free); 2) the effect of power on hinge moments (at various tab angles); and 3) the effect of power on static directional stability with the model operating at high and low angle of attack.

Description of Model

The model used was that of a typical low-wing, single-engine tractor monoplane to one-sixth scale. Consequently, the results of the present tests are most directly applicable to airplanes of the model's general design. Nevertheless, the effects are considered to show qualitatively what may be expected in general, in multiple-engine tractor monoplanes of present day design.

The model essentially consisted of a Northrop Alpha wing and fuselage combined as a low-wing monoplane. A Northrop XBT-1 empennage was used. An N.A.C.A. cowling to one-sixth scale was conventionally mounted over the nine-cylinder radial engine profile, as shown in the photographs, Fig. 1. Landing gear, tail wheel and cockpits with windshields were omitted from the model. A conventional fillet between the fuselage and the upper surface of the wing was employed on all tests. Fig. 2 gives the principal characteristics and dimensions of the model.

The propeller used was a three-bladed fixed-pitch metal propeller, eighteen inches in diameter with each blade profile to one-sixth full scale. The Hamilton Standard 1A1-10 blade form was used except that 10% of the radius was cut off at the tip of each blade. Blades were set at $\beta = 29^{\circ}$ at the three-quarter radius. Power was approximately 1/36 of full-

FRONT VIEW

REAR VIEW

MODEL MOUNTED FOR LONGITUDINAL STABILITY RUNS

TAIL SURFACES

SIDE VIEW

SIDE VIEW

MODEL MOUNTED FOR DIRECTIONAL STABILITY RUNS

FRONT VIEW

FIG. NO. 1

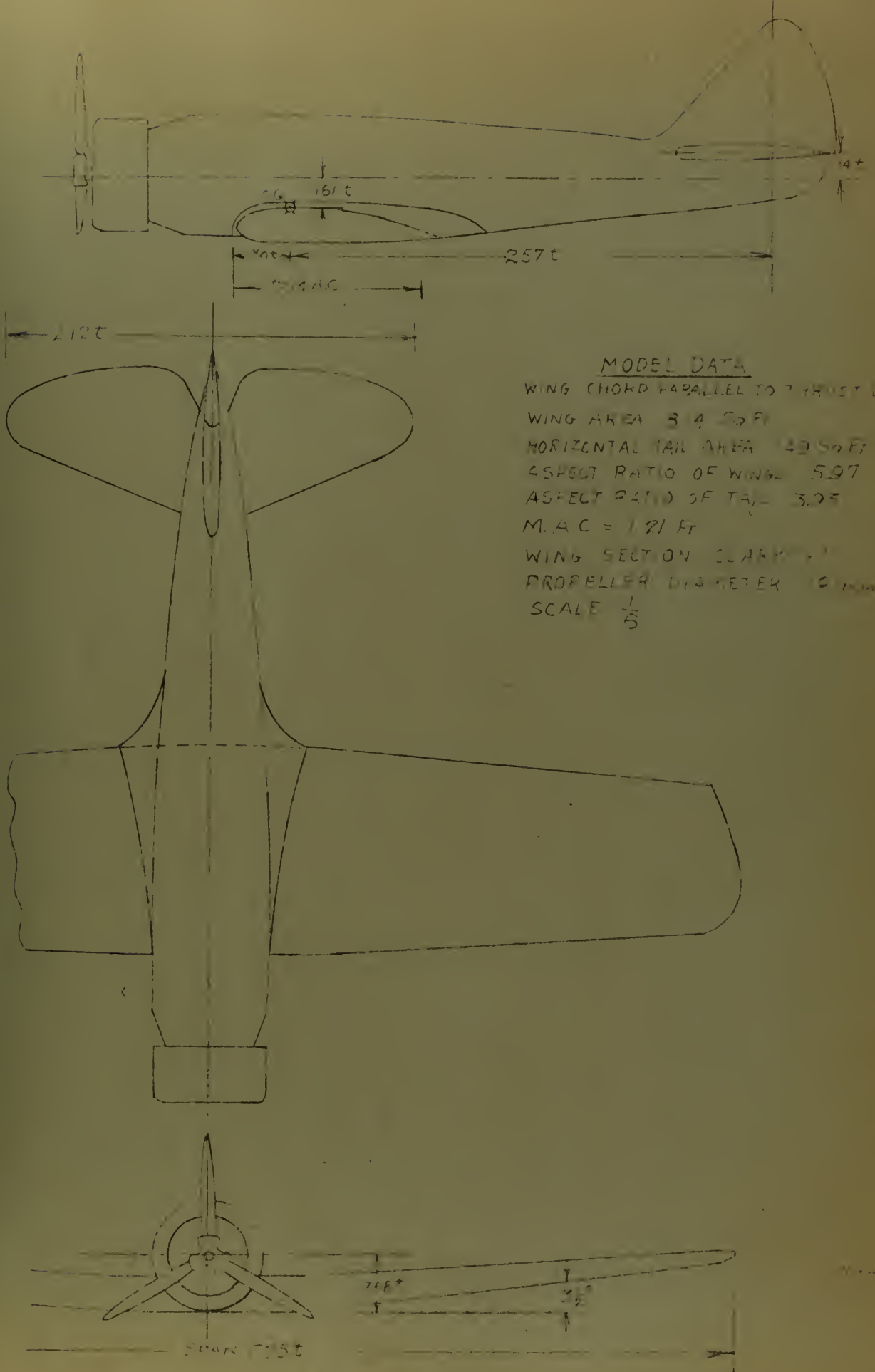
.161 t
.257 t
.212 t
MODEL DATA
WING CHORD PARALLEL TO THRUST LINE
WING AREA 8.4 SQ FT
HORIZONTAL TAIL AREA 1.25 SQ FT
ASPECT RATIO OF WING 5.97
ASPECT RATIO OF TAIL 3.05
M.A.C = 1.21 FT
WING SECTION CLARK Y
PROPELLER DIAMETER 16 INCHES
SCALE 1/5
SPAN 1.95 t

FIG NO. 2

scale power for a 400-450 H.P. engine, (i.e. 432/36 = 12 H.P.), furnished by a three phase, squirrel cage induction motor. Propeller revolutions were six times full-scale revolutions. Thus, the linear velocities of the propeller blade elements equaled full-scale velocities. Since the dimensional homogeneity of the power was preserved, and linear velocities of the model propeller approximated those of a full-scale airplane propeller, the slipstream effects should closely simulate those encountered at full scale.

Explanation: Let $(\ )_m$ refer to properties of the model.

$(\ )$ refer to properties of full-scale airplane.

Note: $D_m = 1/6\ D$; $n_m = 6n$; $V_m = V$; $Q_{c_m} = Q_c$; $\rho_m = \rho$.

Since $P = 2\pi nQ$ and $Q = Q_c \rho V^2 D^3$

$$P_m = 2\pi n_m Q_c \rho V^2 D_m^3$$

$$P = 2\pi n Q_c \rho V^2 D^3$$

Substituting ratios of properties all in terms of $(\ )$

$$\frac{P_m}{P} = \frac{\frac{1}{36} P}{P} = \frac{2\pi \times 6 \times \frac{1}{216}}{2\pi \times 1 \times 1} = \frac{\frac{1}{36}}{1}$$

Further, linear velocity of model's propeller =

$$2\pi \bar{r}_m n_m = 2\pi \frac{1}{6} \bar{r} \times 6n = 2\pi \bar{r} n$$

linear velocity of full-scale propeller =

$$2\pi \bar{r} n = 2\pi \bar{r} n$$

$$\therefore (V_m)_{prop.} = (V)_{prop.}$$

$\left.\begin{array}{l} \bar{r}_m = \frac{1}{6} \bar{r} \\ n_m = 6n \end{array}\right\}$

Description of Apparatus

For the purpose of determining static longitudinal stability (elevator free), the model was mounted as shown in the photographs, Fig. 1. Air velocity, geometrical angle of attack, resultant drag force, lift, and pitching moment, were measured in the conventional manner as set forth in reference 3. The stabilizer was located in the upper middle position with stabilizer angle = +1.3°. The elevator was statically balanced by means of a counterweight housed in the empennage. The counterweight was mounted on an arm secured to the elevator's torque tube at the fuselage centerline. The tabs were mounted on the elevator as shown in sketch 1, and by means of a friction hinge could be securely set at any desired angle. A partial aerodynamic balance of the elevators* was accomplished by extending the leading edge as far forward of the hinge line as possible, without touching the trailing edge of the stabilizer. The angles assumed by the elevator were shown by a pointer attached to the elevator and a dial graduated in degrees which was glued immediately behind the pointer on the rudder's surface. These angles were then observed through a window in the tunnel's side.

* SEE FIG. NO. 7.1

SKETCH 1

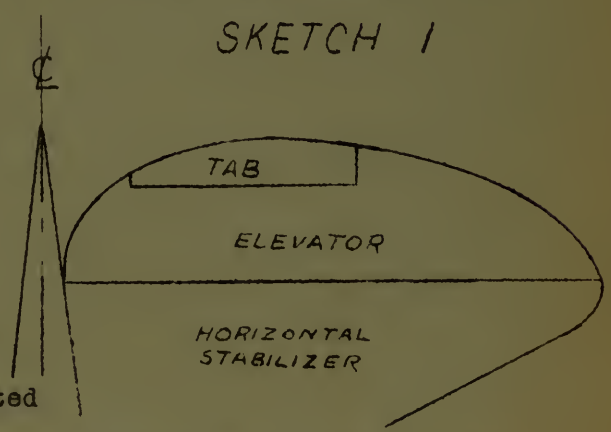

The measurement of the elevator hinge moment coefficient was accomplished by the use of the apparatus shown in sketch 2. Holes were bored in the elevator at a known distance aft of the hinge line (x) and a fine piano wire (gauge W.-M. #29) was secured to the elevator as shown. The upper wire was run vertically out of the tunnel and over a pulley "P" (whose friction was considered negligible) and attached to a weight pan. The lower wire was run through the floor of the tunnel and attached to a weight pan W_2.

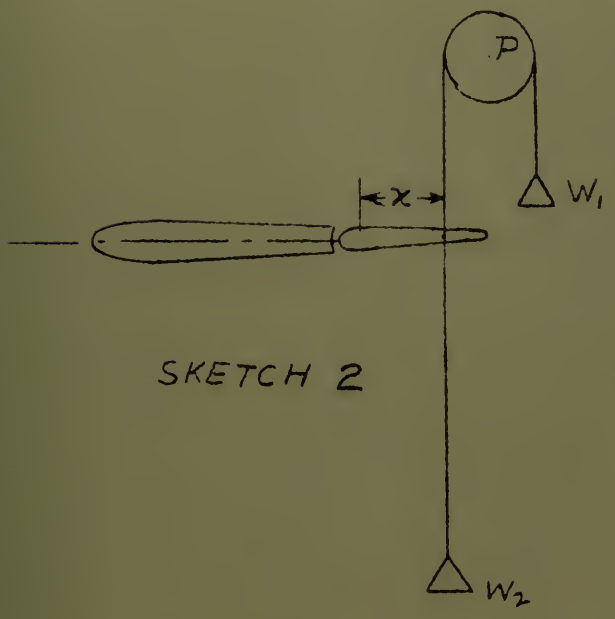

SKETCH 2

By balancing the pans so that the elevator angle is zero prior to a run and then reading the elevator angle assumed during the runs with various ΔW differences between weights in pans W_1 and W_2, the hinge moment coefficient was determined from the formula

$$C_H = \frac{H.M.}{qSt} = \frac{1000\ \Delta W\ (\text{in Kg.})\ \cos\sigma\ x\ (x)}{q \times \text{area elevator aft of hinge} \times \text{mean chord aft of hinge}}$$

where $\sigma = \alpha_u + s + e$ (SEE SKETCH 3)

paying proper heed to signs.

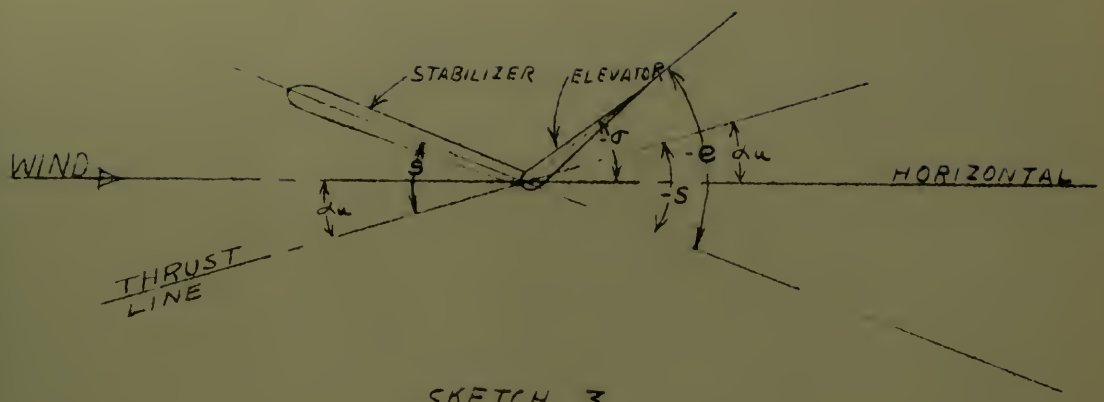

SKETCH 3

The measurement of the yawing moment coefficient was accomplished by mounting the model in the wind tunnel in the normal manner for measuring yawing moment via the pitching moment balance. (See photograph). Wires of proper length were provided for adjusting the model to two angles of attack, viz. a low angle of attack ($\alpha_u = -2^\circ$) for simulating high speed conditions and a higher angle of attack ($\alpha_u = 8^\circ$) for simulating low speed conditions. The model's rudder could be fixed at various values of rudder angle "r" from 0 to 25° on either side in increments of five degrees each. For this portion of the test, the elevator was locked at zero position and the tabs were set at zero angle.

Methods of Measuring Power

1) The power parameter "tan θ" was employed in connection with that portion of the experiment dealing with the effect of power on static longitudinal stability (elevator free). A brief description of this parameter is herewith presented. For more detailed presentation see Part 2 of reference 1.

Given an airplane in unaccelerated flight moving along a flight path parallel to the thrust line.

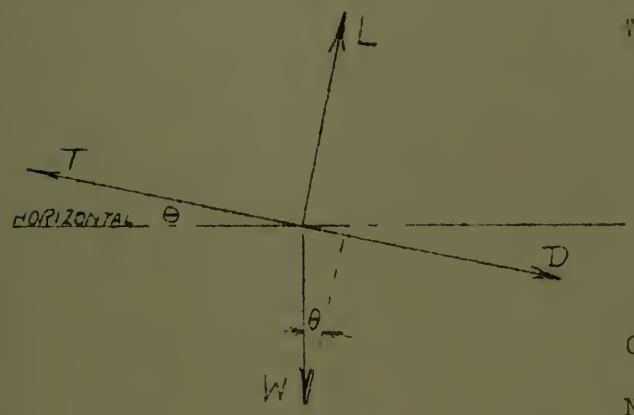

SKETCH 4

Write T = Thrust

D = Drag

θ = Angle of Climb

W = Weight

L = Lift

Observe $T = D + W \sin \theta$

Net thrust $= T - D = W \sin \theta$

$L = W \cos \theta$

$$\frac{T - D}{L} = -\frac{C_R}{C_L} = \frac{W \sin \theta}{W \cos \theta} = \tan \theta$$

Thus, it is seen that the tangent θ, where θ is the angle of climb or glide, is a measure of the amount of thrust developed by the propeller. C_R and C_L are obtained directly from wind tunnel data and the values of tan θ are readily obtained. "Power on" results are given in terms of C_M vs. C_L for various values of tan θ.

2) The power parameter, herein designated as "$\overline{R}$", was employed in connection with that portion of the tests dealing with the effect of power on hinge moments (elevator free) and the effect of power on static directional stability. This power parameter was employed in preference to tan θ in this portion of the tests, due to the fact that no accurate means was at hand to determine "C_R" with the type of rigging employed. A brief derivation of the power parameter "$\overline{R}$" is herewith presented.

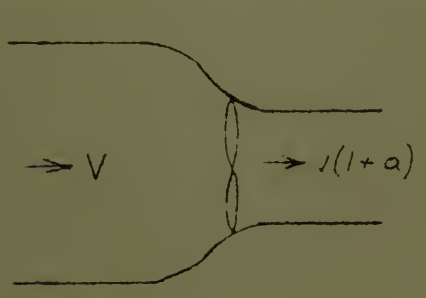

SKETCH 5

From Froude Theory

$$T = A\rho V^2 a\left(1 + \frac{a}{2}\right)$$

where A = area of disc

T = thrust

Meaning of V and a is shown in sketch.

By definition (Weick p. 87)

$$T = T_c \rho V^2 D^2$$

Observe, from sketch, $\frac{V(\text{slipstream})}{V(\text{at } \infty)} = \frac{V(1+a)}{V} = \frac{1+a}{1}$

Write $\frac{V(\text{slipstream})}{V(\text{at } \infty)} = \overline{R} = 1 + a$; i.e. $a = \overline{R} - 1$

Then $T_c \rho V^2 D^2 = A\rho V^2 (\overline{R} - 1)\left(1 + \frac{\overline{R} - 1}{2}\right)$

$$T_c = \frac{\pi}{4}(\overline{R} - 1)\,\frac{\overline{R} + 1}{2} = \frac{\pi}{8}(\overline{R}^2 - 1)$$

$$\overline{R}^2 = \frac{8}{\pi} T_c + 1$$

$$\overline{R} = \sqrt{\frac{8}{\pi} T_c + 1}$$

The Q_c, T_c vs. J curve for $\beta = 29^\circ$ at 3/4 radius is presented in Fig. 3. The propeller revolutions were counted by means of a system consisting of a pendulum actuated multiple relay circuit which counted the revolutions made over a ten-second period. Calibration was accomplished by reference to a crystal-controlled 50 cycle current, at the beginning of each run.

"$\overline{R}$" will, of course, vary slightly with angle of inclination of thrust line to direction of undisturbed airflow. Experimental results show that the error introduced due to this inclination is negligible, as seen in the experimental curve in adjoining sketch 6.

SKETCH 6

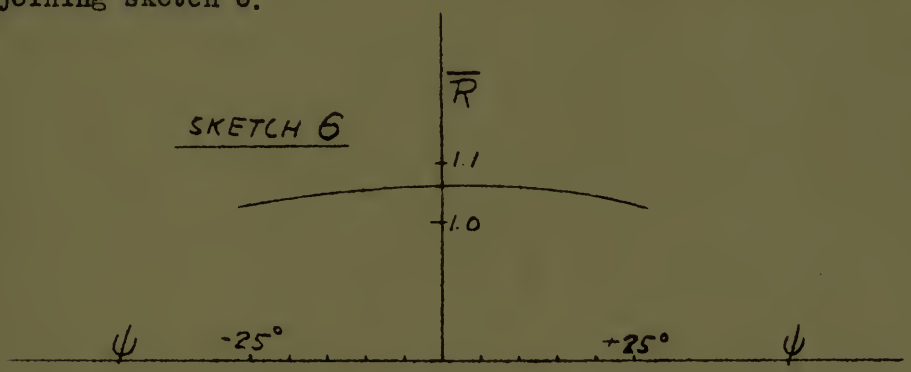

Range of Power

The range of power used was sufficient to cover the flying range for an airplane of a type similar to that of the model. The method of determining this range was identical to that outlined in reference 1.

In order to show the relation between $\overline{R}$ and tangent θ, a power available, power required curve is shown plotted in Fig. 3.1, with various values of $\overline{R}$ and tangent θ spotted in at proper points.

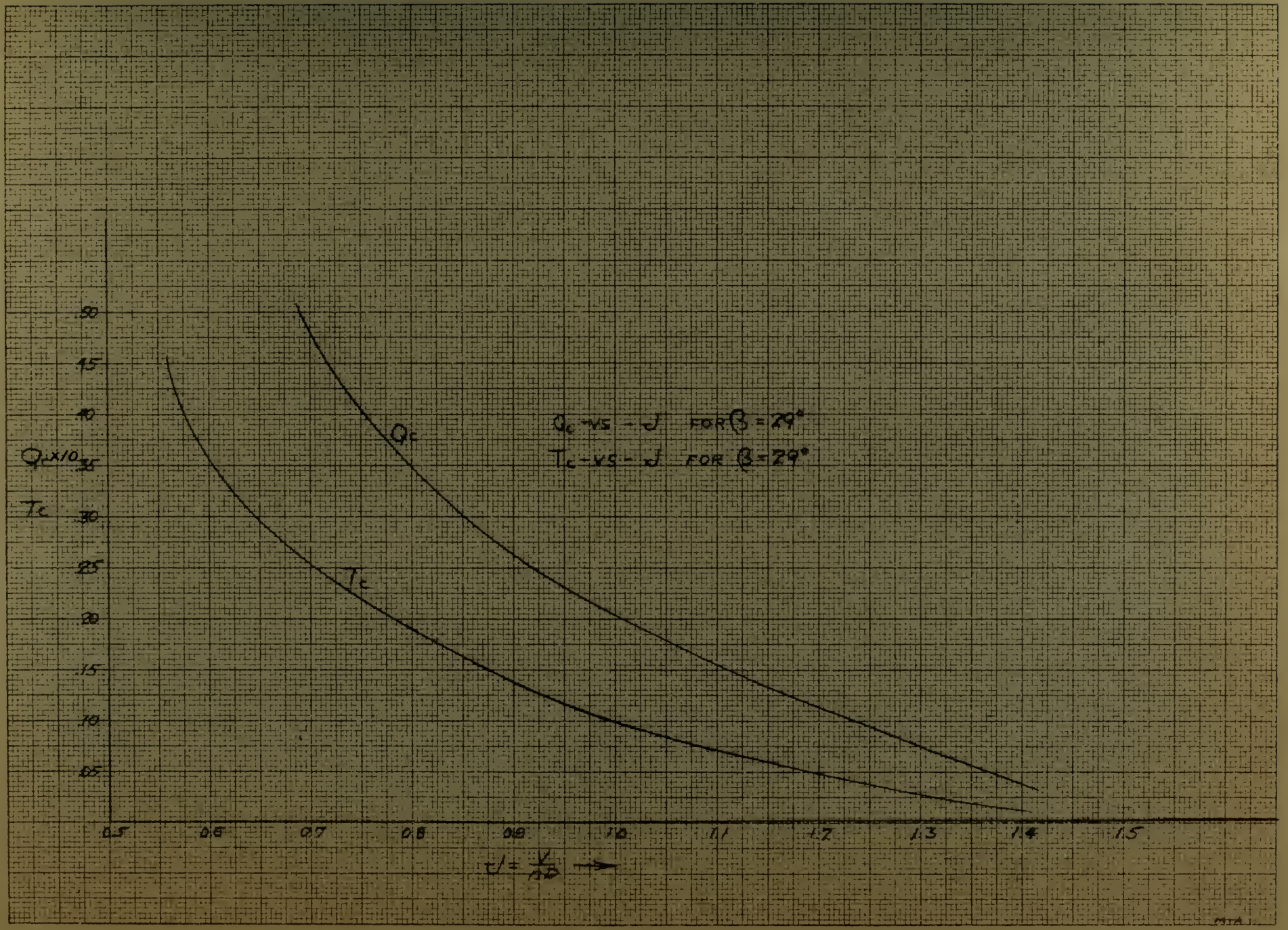
Q_c -VS - J FOR $\beta = 29°$
T_c -VS - J FOR $\beta = 29°$
Q_c
T_c
$Q_c \times 10$
T_c
50
45
40
35
30
25
20
15
10
05
0.5
0.6
0.7
0.8
0.9
1.0
1.1
1.2
1.3
1.4
1.5
$J = \frac{V}{nD}$ →

FIG. NO. 3

COMPARISON OF POWER PARAMETERS TANGENT θ AND $\bar{R}$

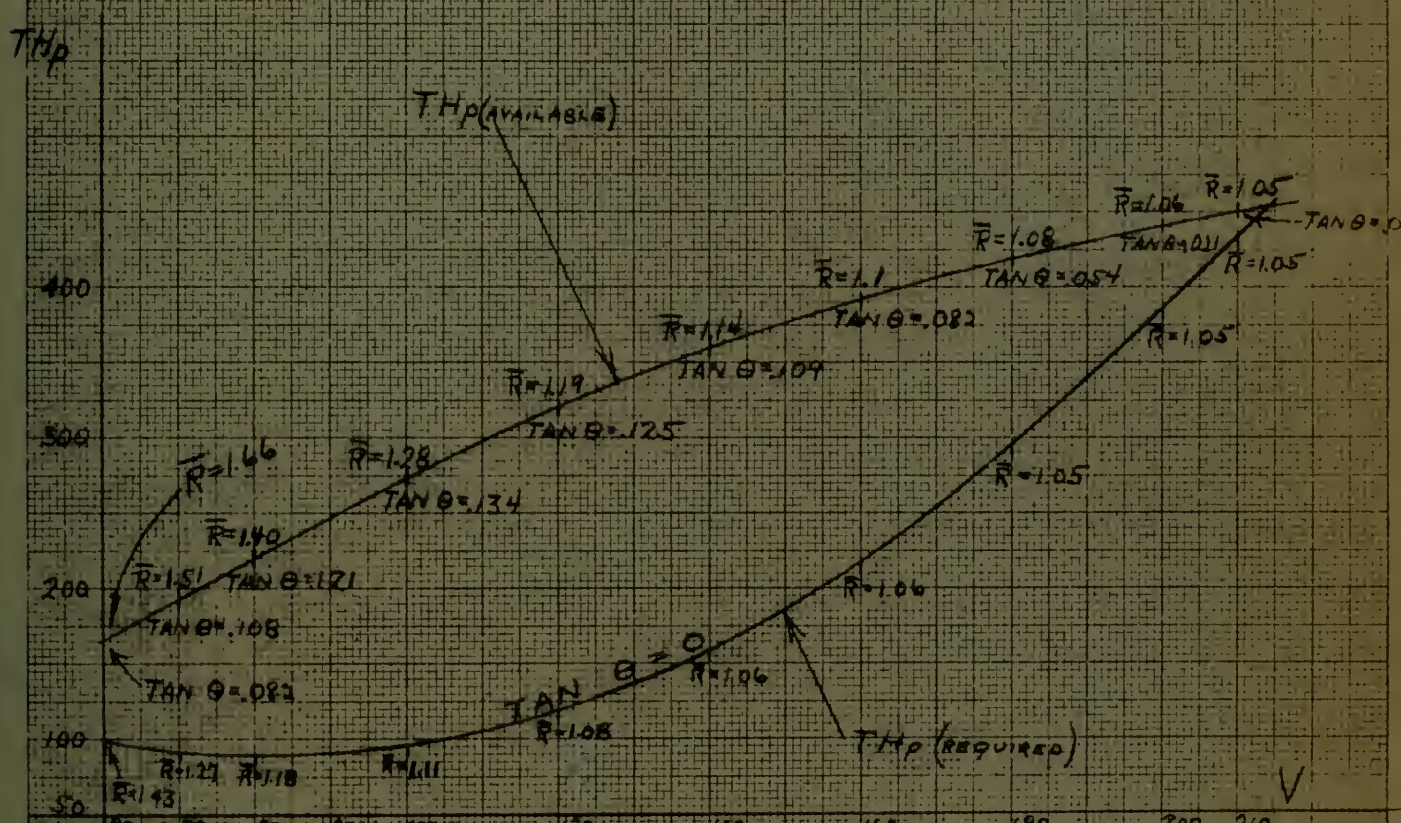

ALL CALCULATIONS BASED UPON AIRPLANE SIMILAR TO POWER MODEL

M+A

FIG. NO. 3.1

Static Longitudinal Stability (Elevator Free)

The curves showing the effect of power on static longitudinal stability (elevator free), are shown in Fig. 4. A separate family of curves is drawn for each tab angle. Each family of curves shows the effects of power ranging from tan θ = -0.05 to tan θ = +0.15.

The effect of power on static longitudinal stability for tab angles of +20 and +30 degrees was investigated but showed such small variation from the effects noted for $+10^{\circ}$ tab angle, that curves for the former angles are not included in this report.

The singular, wavy character of the "power on" curves is explained as follows: Let C_{M_t} be plotted against C_L for various fixed elevator angles. Now, for a single tab angle, with elevator free, as C_L varies, the elevator angle assumes various values, giving a resulting C_{M_t} vs. C_L curve, as shown in sketch 7. This C_{M_t} combined with the moment coefficient due to wing and fuselage alone (at various corresponding powers), will produce an overall C_M vs. C_L curve of a similar wavy nature. The variation in elevator angle responsible for this effect is due to 1) interference effects, 2) variation in α, and 3) downwash.

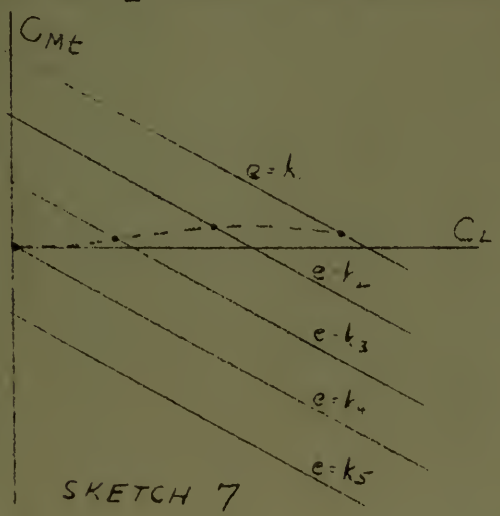

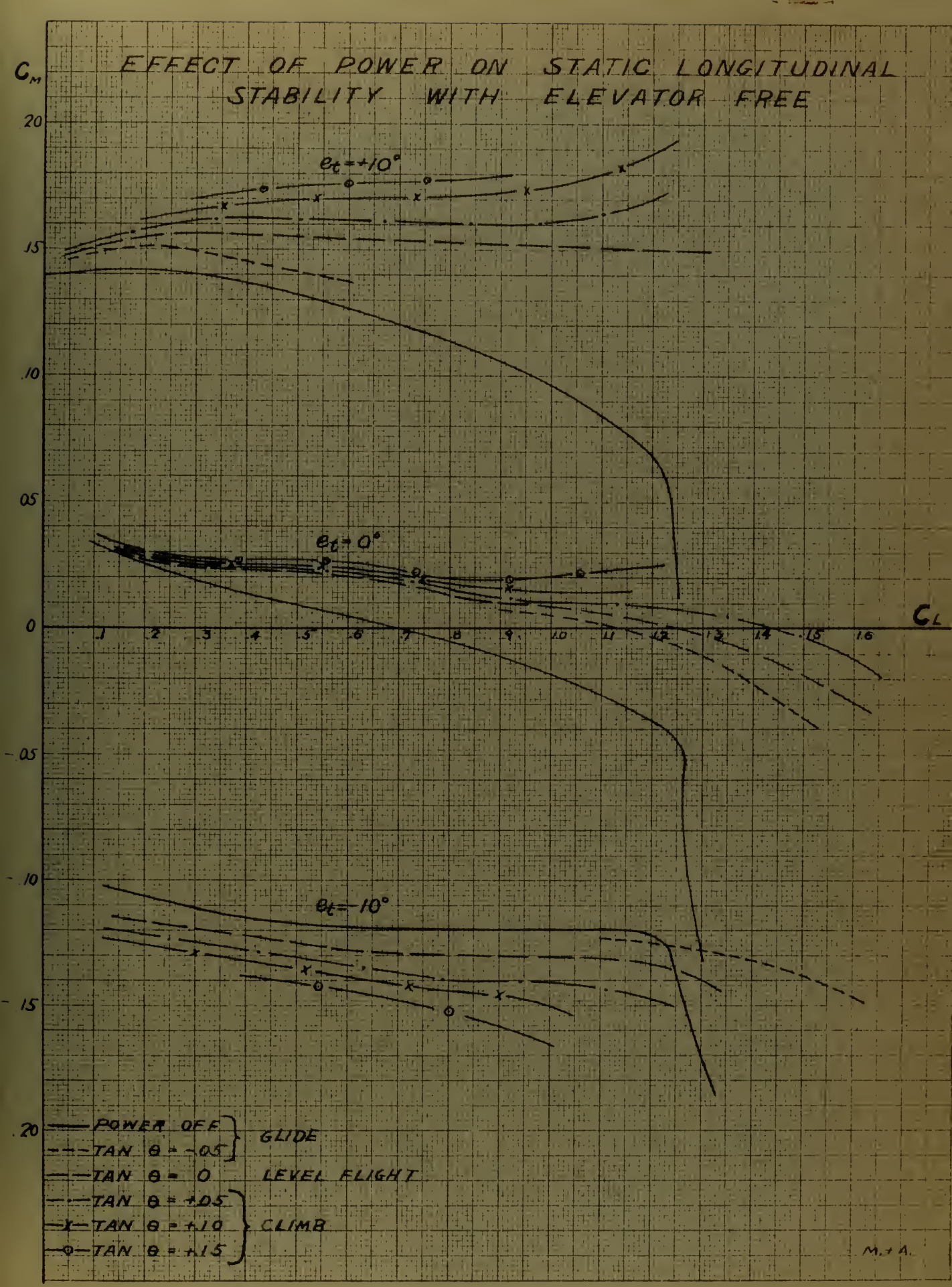
EFFECT OF POWER ON STATIC LONGITUDINAL STABILITY WITH ELEVATOR FREE
C_M
C_L
$e_t = +10°$
$e_t = 0°$
$e_t = -10°$
.20
.15
.10
.05
0
-.05
-.10
-.15
.1
.2
.3
.4
.5
.6
.7
.8
.9
1.0
1.1
1.2
1.3
1.4
1.5
1.6
POWER OFF
TAN θ = -.05
GLIDE
TAN θ = 0
LEVEL FLIGHT
TAN θ = +.05
TAN θ = +.10
TAN θ = +.15
CLIMB
M. + A.

FIG. NO. 4

CALIFORNIA INSTITUTE OF TECHNOLOGY
PASADENA, CALIFORNIA
12 June, 1937

From : Lieutenant S.S.Miller, U.S.Navy.

To : Head of Postgraduate School

Subject : Correction to Thesis.

Reference (A)." Thesis --Wind Tunnel Tests of a low wing monoplane with propeller running," by Lts.Miller &Albach.

1. Reference (A) was forwarded to the Postgraduate School on a recent date. In the interim the following error has been discovered:

At the bottom of page 17 in the formula for C_{M_t} all aspect ratios (AR and AR_t) should be multiplied by the quantity "π". The formula will then read

$$C_{M_t} = -\eta_t \frac{l}{t} \frac{S_t}{S} \left[\frac{1 - \frac{a_0}{\pi AR}}{1 + \frac{a_0}{\pi AR_t}} C_L - \frac{a_0}{1 + \frac{a_0}{\pi AR_t}} \alpha_d \right]$$

Similarly, at the top of page 18, the corrected formula for $\frac{dC_{M_t}}{dC_L}$ should read $\frac{dC_{M_t}}{dC_L} = -\eta_t \frac{l}{t} \frac{S_t}{S} \left[\frac{1 - \frac{a_0}{\pi AR}}{1 + \frac{a_0}{\pi AR_t}} \right]$

And in the middle of page 18 the corrected formula for C_{M_t}' should read

$$C_{M_t}' = -\eta_t \frac{l}{t} \frac{S_t}{S} \left[K \frac{1 - \frac{a_0}{\pi AR}}{1 + \frac{a_0}{\pi AR_t}} C_L - K \frac{a_0}{1 + \frac{a_0}{\pi AR_t}} \alpha_d \right]$$

S.S.Miller

S S Miller

18940

Let us now turn our attention to Fig. 5, which shows static longitudinal stability without tail (i.e. $C_{M_{W+F}}$ vs. C_L) for various powers. (Note: $C_{M_{W+F}} = C_M$ due to presence of wing and fuselage alone). Now, in order to find the effects of slipstream and tab on tail moments, the values of the moment coefficient for wing and fuselage alone (for various powers) were subtracted from the values obtained for the complete airplane model (for corresponding powers).

Values thus obtained were plotted and straight lines were faired through the points thus obtained below a lift coefficient of 1.0. These faired curves of C_{M_t} vs. C_L are shown in Fig. 6.

From a study of the curves in Fig. 6, it is seen that the effect of power on static longitudinal stability (elevator free) consists of two parts: 1) a change in the slope of the tail moment coefficient curve, dC_{M_t}/dC_L, and 2) a change in the intercept for any given change of tab angle from the neutral position.

For power off

$$C_{M_t} = -\eta_t \frac{\ell_t}{\bar{c}} \frac{S_t}{S} \left[\frac{1 - \frac{a_o}{AR}}{1 + \frac{a_o}{AR_t}} C_L - \frac{a_o}{1 + \frac{a_o}{AR_t}} \alpha_d \right]$$

EFFECT OF POWER ON STATIC LONGITUDINAL STABILITY WITHOUT TAIL

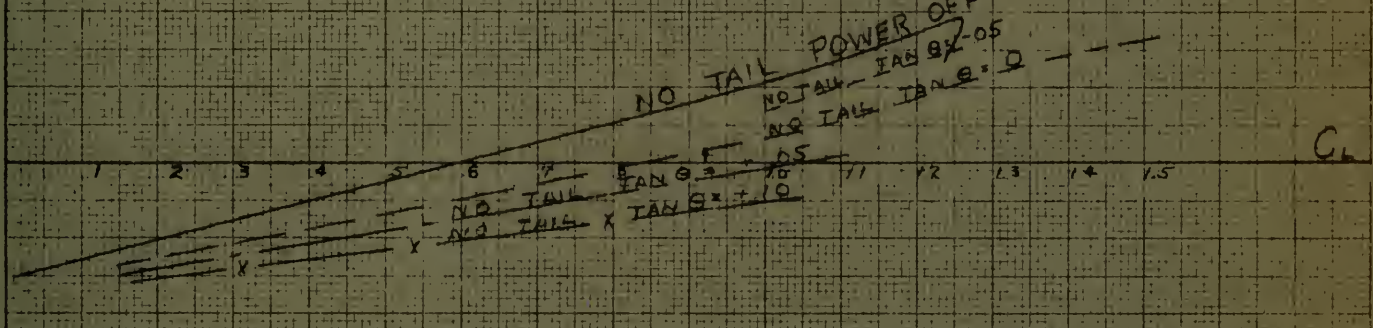

FIG NO. 5

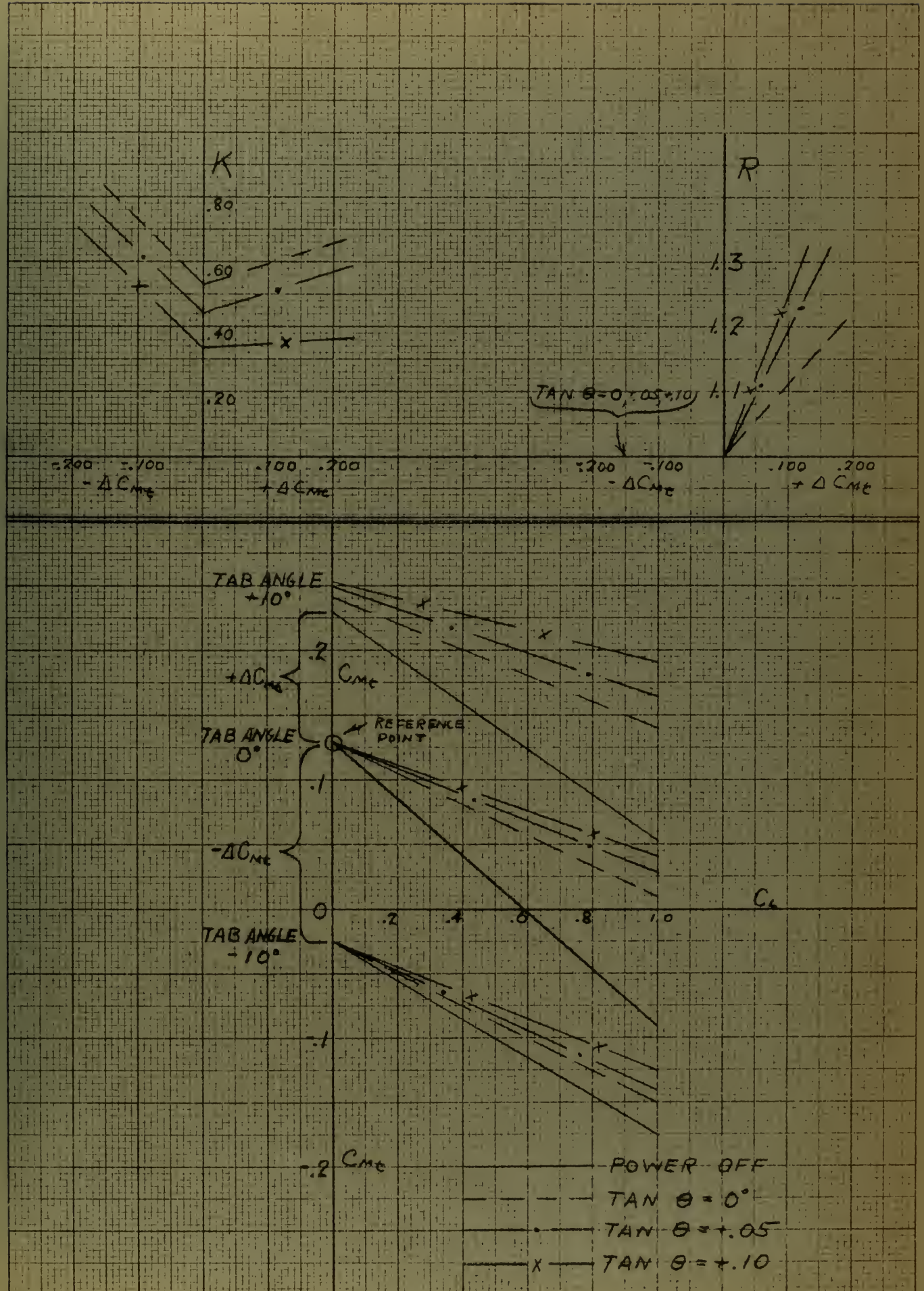
K
.80
.60
.40
.20
-.200
-.100
.100
.200
$-\Delta C_{mc}$
$+\Delta C_{mc}$
R
1.3
1.2
1.1
TAN θ=0, .05, .10
-.200
-.100
.100
.200
$-\Delta C_{mc}$
$+\Delta C_{mc}$
TAB ANGLE +10°
$+\Delta C_{mc}$
.2
C_{mc}
REFERENCE POINT
TAB ANGLE 0°
.1
$-\Delta C_{mc}$
0
TAB ANGLE -10°
-.1
-.2
C_{mc}
.2
.4
.6
.8
1.0
C_L
POWER OFF
TAN θ = 0°
TAN θ = +.05
TAN θ = +.10

FIG NO. 6

$$\frac{dC_{M_t}}{dC_L} = -\eta_t \frac{\ell}{t}\frac{S_t}{S}\left[\frac{1 - \frac{a_o}{AR}}{1 + \frac{a_o}{AR_t}}\right]$$

Let $\frac{dC_{M_t}'}{dC_L}$ = Slope, power on, for tab angle in question.

$\frac{dC_{M_t}}{dC_L}$ = Slope, power off, for tab angle in question.

Adopting notations following those used in reference 4, write

$$K = \frac{\frac{dC_{M_t}'}{dC_L}}{\frac{dC_{M_t}}{dC_L}}$$

and $R = \frac{\Delta C_{M_t}'}{\Delta C_{M_t}} = \frac{\text{Change in tail moment coefficient due to tab angle, power on (AT } C_L = 0)}{\text{Change in tail moment coefficient for same tab angle, power off (AT } C_L = 0)}$

Then $C_{M_t}' = -\eta_t \frac{\ell}{t}\frac{S_t}{S}\left[K\frac{1 - \frac{a_o}{AR}}{1 + \frac{a_o}{AR_t}} C_L - R\frac{a_o}{1 + \frac{a_o}{AR_t}} \alpha_d\right]$

In explanation, ΔC_{M_t} = the difference between the tail moment coefficient for a given tab setting at "power off" and the tail moment coefficient for tab angle zero, "power off", both taken at $C_L = 0$.

$\Delta C_{M_t}'$ = the difference between the tail moment coefficient for a given tab setting, "power on", (various values), and the tail moment coefficient for tab angle zero, power off, both taken at $C_L = 0$.

In Fig. 6, values of K and R for various amounts of power and for different tab angles are plotted vs. ΔC_{M_t}.

It is obvious that K and R will also vary with the location of the horizontal stabilizer. This variation was not investigated in this report but was covered in reference 4.

For purposes of comparing the values of K and R for elevator free and elevator fixed, Fig. 6.1 is included in this report, this figure being an exact copy of the one computed and plotted by Bolster in reference 4.

In order to make use of these data and obtain the pitching moment coefficient of the complete airplane model for "power on", proceed as follows:

1) Let (-) correspond to power off values.

   (-)' correspond to power on values.

2) Obtain C_M vs. C_L curves for model from wind tunnel tests. (It is assumed that model has no power plant nor propeller installed).

3) Obtain $C_{M_{(no\ tail)}}$ vs. C_L curves from wind tunnel results.

4) Obtain C_{M_t} by taking difference between 3) and 2) and plot resulting C_{M_t} vs. C_L curves.

5) Obtain K and R as described above and compute and plot C_{M_t}'.

6) Refer to Fig. 6.2, replotted from Bolster (reference 4), [AND PAGES 20 & 21] which gives method of determining $C_{M_{(no\ tail)}}$ with power on = $C_{M_{(no\ tail)}}'$.

7) Obtain final result $C_M' = C_{M_{(no\ tail)}}' + C_{M_t}'$.

SLOPE POWER ON = K × SLOPE POWER OFF

MOMENT CHANGE POWER ON = R × MOMENT CHANGE POWER OFF

$\Delta C_{M_\epsilon} = R \times \Delta C_{M_\epsilon}$

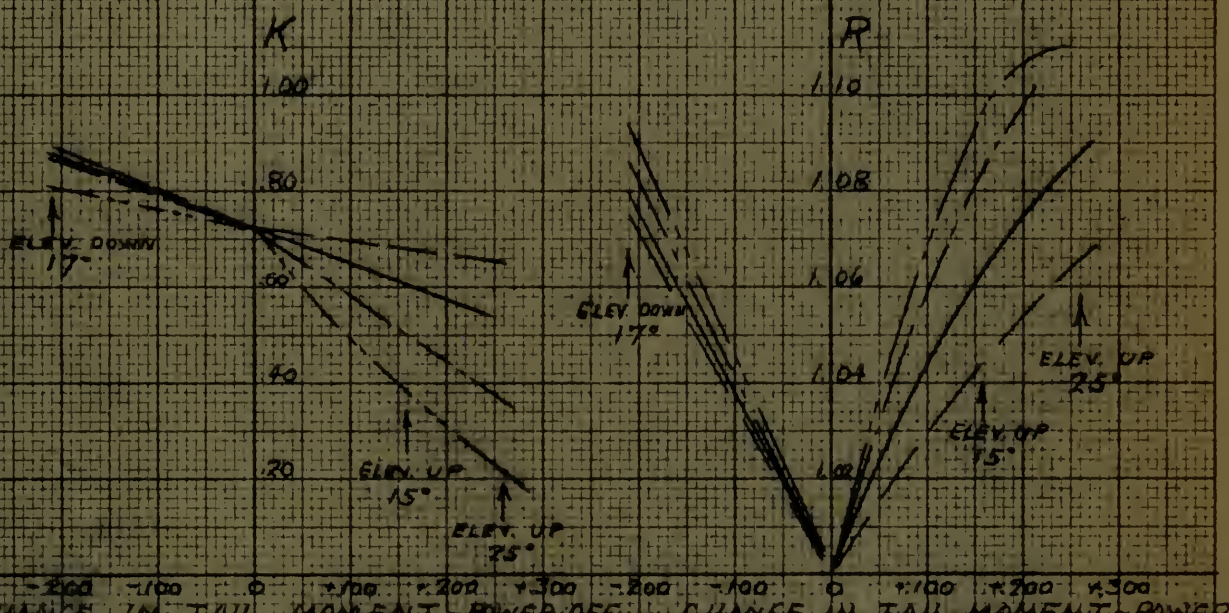

TAN Θ = -.05

TAN Θ = 0 (LEVEL FLIGHT)

TAN Θ = +.05

TAN Θ = +.10

FIG. NO. 6.1

CORRECTION TO $C_{M\,NO\,TAIL}$ FOR POWER

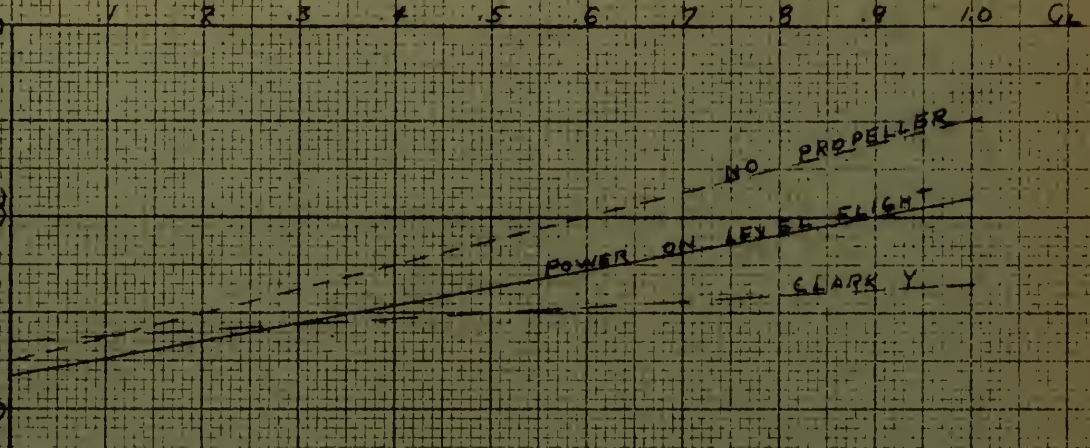

POWER OFF

$$C_{M\,NO\,TAIL} = C_{M_W} + C_{M_P} = C_{M_o} + \Delta C_{M_o} + \left(\frac{d}{c} - \frac{h}{c}\right) C_L + \Delta F\, C_L$$

FROM ABOVE $\Delta C_{M_o} = -.010$

$$\Delta F = +.097 - \left(\frac{d}{c} - \frac{h}{c}\right) = +.097 - .050 = +.047$$

POWER ON

$$C_{M\,NO\,TAIL} = C'_{M_W} + C'_{M_P} = C_{M_o} + \Delta C_{M_o} + \Delta C'_{M_o} + \left(\frac{d}{c} - \frac{h}{c} + \frac{\Delta h}{c}\right) C_L + \Delta F C_L + C_{M_{ch}}$$

$$= C_{M_{W+P}} + C_{M_{ch}} + \Delta C'_{M_o} + \frac{\Delta h}{c}$$

VALUES OF $\Delta h/c$ AND $\Delta C'_{M_o}$ VARY WITH POWER.
VALUES OBTAINED ARE PLOTTED BELOW

$C_{M_{ch}} = \dfrac{\text{MOMENT DUE TO THRUST}}{q\,S\,c}$, MUST BE INCLUDED IN CALCULATING $C'_{M_{W+P}}$
FOR ANOTHER AIRPLANE, USING $T = \dfrac{D}{\cos\alpha}$

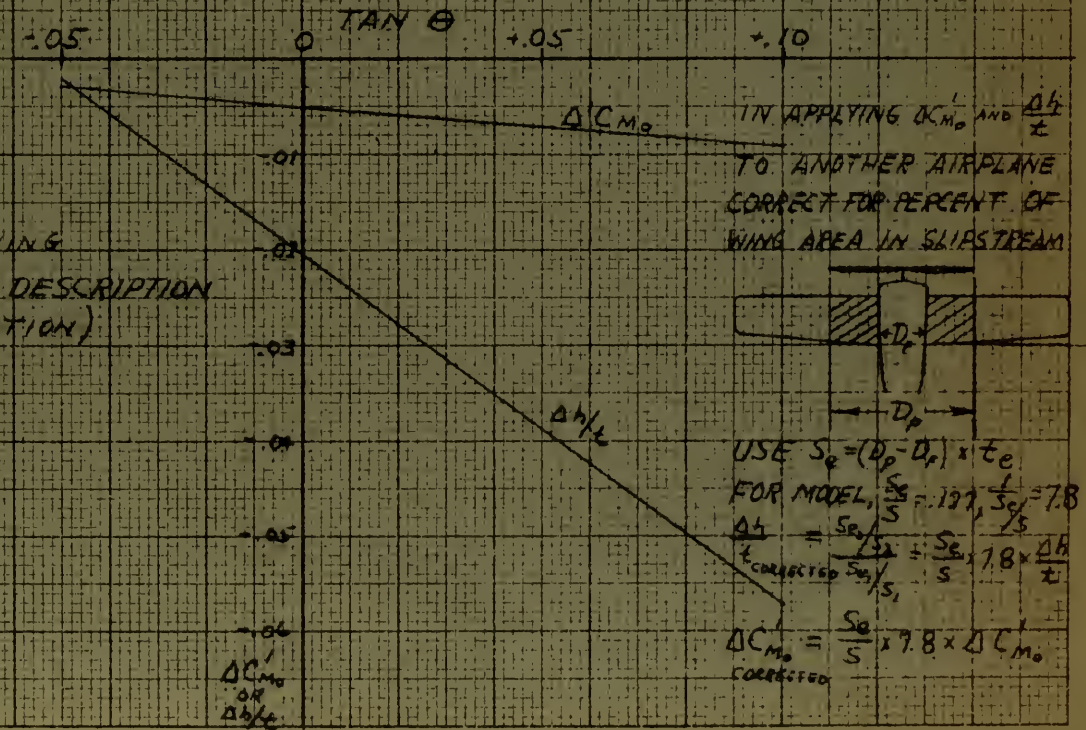

(SEE FOLLOWING PAGES 20 + 21 FOR DESCRIPTION OF COMPUTATION)

IN APPLYING $\Delta C'_{M_o}$ AND $\frac{\Delta h}{c}$ TO ANOTHER AIRPLANE CORRECT FOR PERCENT OF WING AREA IN SLIPSTREAM

USE $S_e = (D_p - D_f) \times t_e$

FOR MODEL, $\frac{S_e}{S} = .127$, $\frac{1}{S_e/S} = 7.8$

$$\frac{\Delta h}{c}_{\text{CORRECTED}} = \frac{S_e/S_2}{S_e/S_1} \frac{\Delta h}{c} = \frac{S_e}{S} \times 7.8 \times \frac{\Delta h}{c}$$

$$\Delta C'_{M_o\,\text{CORRECTED}} = \frac{S_e}{S} \times 7.8 \times \Delta C'_{M_o}$$

FIG. NO. 6.2

The wing and fuselage moment coefficients were determined together, both for power off and power on.

$$C_{M_F} + C_{M_W} = C_{M_o} + \Delta C_{M_o} + \left(\frac{d}{t} - \frac{h}{t}\right) C_L + \Delta F C_L$$

In Fig. 6.2, C_{M_o} for a Clark Y section is plotted.

At $C_L = 0$, $\quad C_{M_o} = -.065$

But at $C_L = 0$, $\quad C_{M_F} + C_{M_W} = -.075$

Therefore $\Delta C_{M_o} = -.010$

$\frac{d}{t} - \frac{h}{t} = .30 - .25 = .050$ since center of gravity was assumed to be at .30t from leading edge.

As shown in Fig. 6.2, $\Delta F = +.047$

$$C_{M_{W+F}} = C_{M_o} - .010 + \left(\frac{d}{t} - \frac{h}{t} + .047\right) C_L$$

Considering "power on" effects, write:

$$C_{M_{W+F}}' = C_{M_{th}} + C_{M_{W+F}} + \Delta C_{M_o}' + \frac{\Delta h}{t} C_L$$

Where $C_{M_{th}}$ = Moment Coefficient due to thrust = $\frac{T \times \text{Vert. Height of T above C.G.}}{qSt}$

and $T = \frac{D}{\cos \omega}$

$\Delta C_{M_o}'$ = change in C_{M_o} due to power

$\frac{\Delta h}{t}$ may be considered as a change in the location of the aerodynamic center due to power.

Values of $C_{M_{th}}$ were calculated at $C_L = 0$ and $C_L = 1.0$, and the increments not due to thrust, $\Delta C_{M_o}'$ and $\frac{\Delta h}{t}$ were obtained as follows:

a) $\Delta C_{M_o}'$ is the increment of wing-fuselage moment coefficient at $C_L = 0$ due to power, except for that due to thrust.

$$\text{Thus } \Delta C_{M_o}' = C_{M_o}' - C_{M_{th}(\text{at } C_L = 0)} - C_{M_{W+F}(\text{at } C_L = 0)}$$

b) $\frac{\Delta h}{t}$ is the change in slope of the wing-fuselage moment coefficient curve due to power, except for that due to thrust.

$$\text{Thus } \frac{\Delta h}{t} = \frac{dC_{M_{W+F}}'}{dC_L} - \frac{dC_{M_{W+F}}}{dC_L} - \frac{dC_{M_{th}}}{dC_L}$$

Fig. 6.2 gives the results obtained as a function of tan θ. A method of predicting $C_{M_{W+F}}'$ for other airplanes is also given.

A calculated curve of wing and fuselage moment coefficient, power on, versus angle of attack was also prepared.

The Effect of Power on Hinge Moments
(at various tab angles)

Reference to the C_H vs. e curves, shown in Figs. 8-17 inclusive, shows that, in general, the hinge moment coefficient is increased by the presence of the slipstream.

The angles of attack investigated were α_u = -2-1/2°; 0°; +8°; and +16°. The tab angles investigated were e_t = -10°; 0°; 10°; 20° and 30°. Powers investigated are defined in terms of the "$\overline{R}$" parameter of power, whose meaning has been explained in an earlier portion of this paper, under the subdivision "Methods of Measuring Power".

(FOR AERODYNAMIC BALANCE OF ELEVATORS SEE FIG. NO. 7.1)

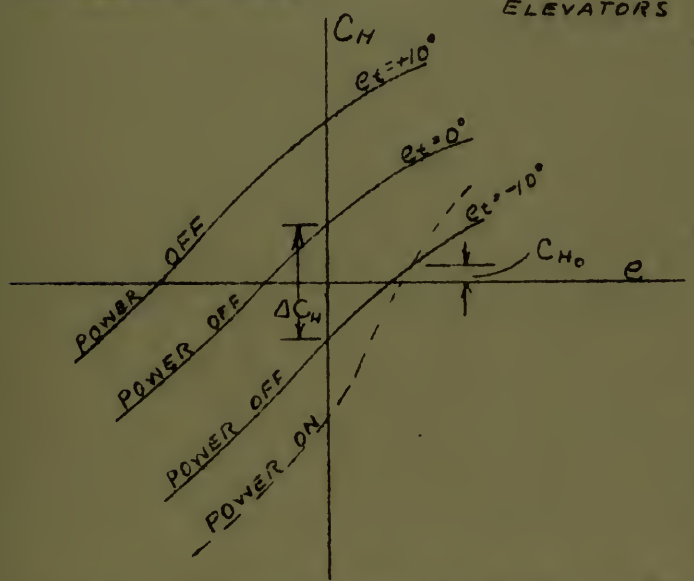

Define C_H' = C_H with power (see Fig. 7)

C_H = C_H without " " " "

$\Delta C_H = C_{H(e_t = k,\ e = 0,\ \text{Power} = 0)} - C_{H(e_t = 0,\ e = 0,\ \text{Power} = 0)}$

(See adjoining sketch).

C_{H_o} = C_H where C_H' = C_H for tab angle in question. (See adjacent sketch).

1) Plot $(C_H' - C_{H_o})$ vs. $(C_H - C_{H_o})$ for $\overline{R}$ = constant. (Fig. 19).

2) It appears that we get straight lines so that

$$(C_H' - C_{H_o}) = (C_H - C_{H_o})\, f(\overline{R})$$

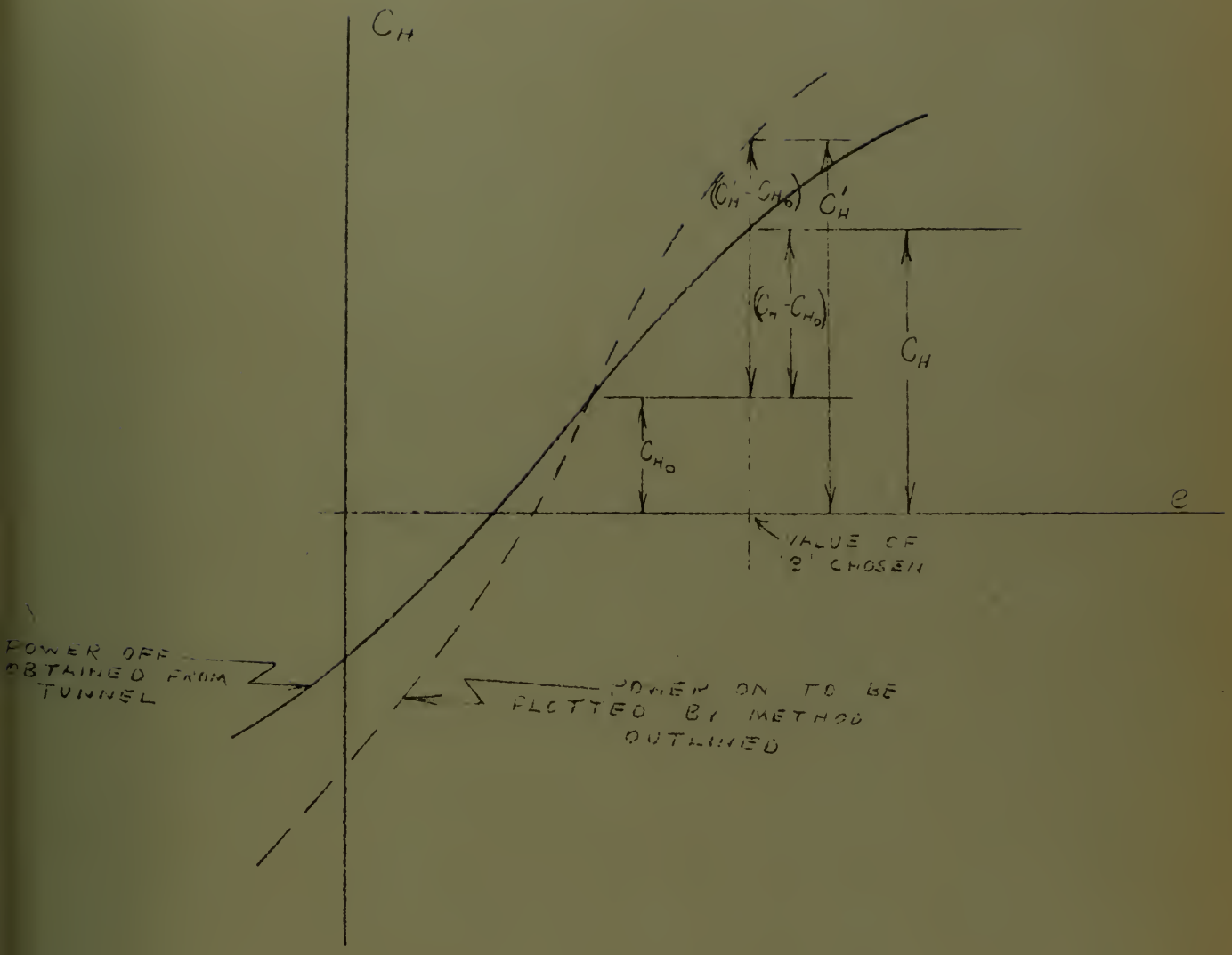
C_H
$(C_H' - C_{H_0})$
C_H'
$(C_H - C_{H_0})$
C_H
C_{H_0}
α
VALUE OF α' CHOSEN
POWER OFF OBTAINED FROM TUNNEL
POWER ON TO BE PLOTTED BY METHOD OUTLINED

FIGURE NO. 7

DIAGRAM OF ELEVATOR SHOWING PERCENTAGE OF AERODYNAMIC BALANCE

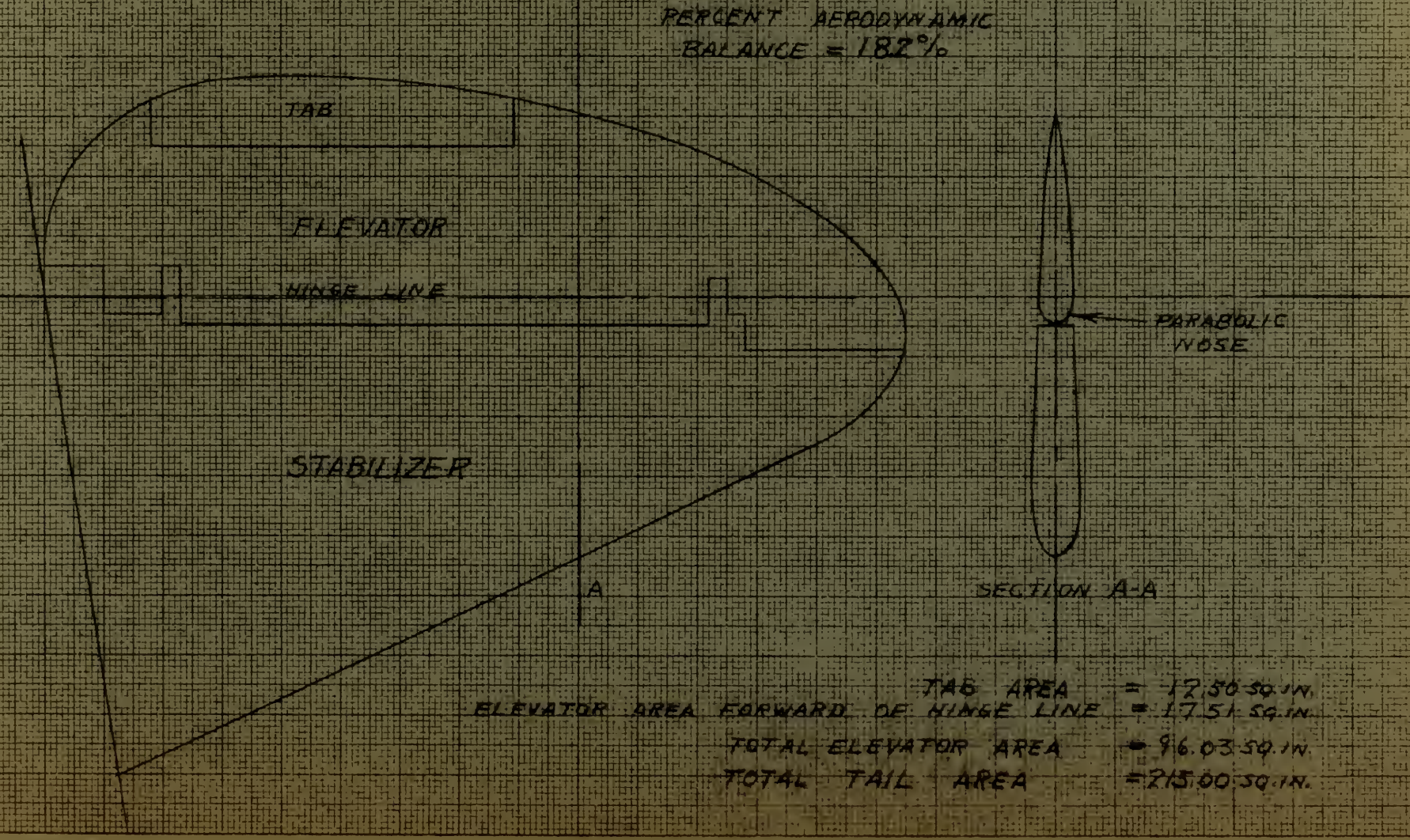

TAB AREA = 12.50 SQ. IN.
ELEVATOR AREA FORWARD OF HINGE LINE = 17.51 SQ. IN.
TOTAL ELEVATOR AREA = 96.03 SQ. IN.
TOTAL TAIL AREA = 215.00 SQ. IN.

FIG. NO. 7.1

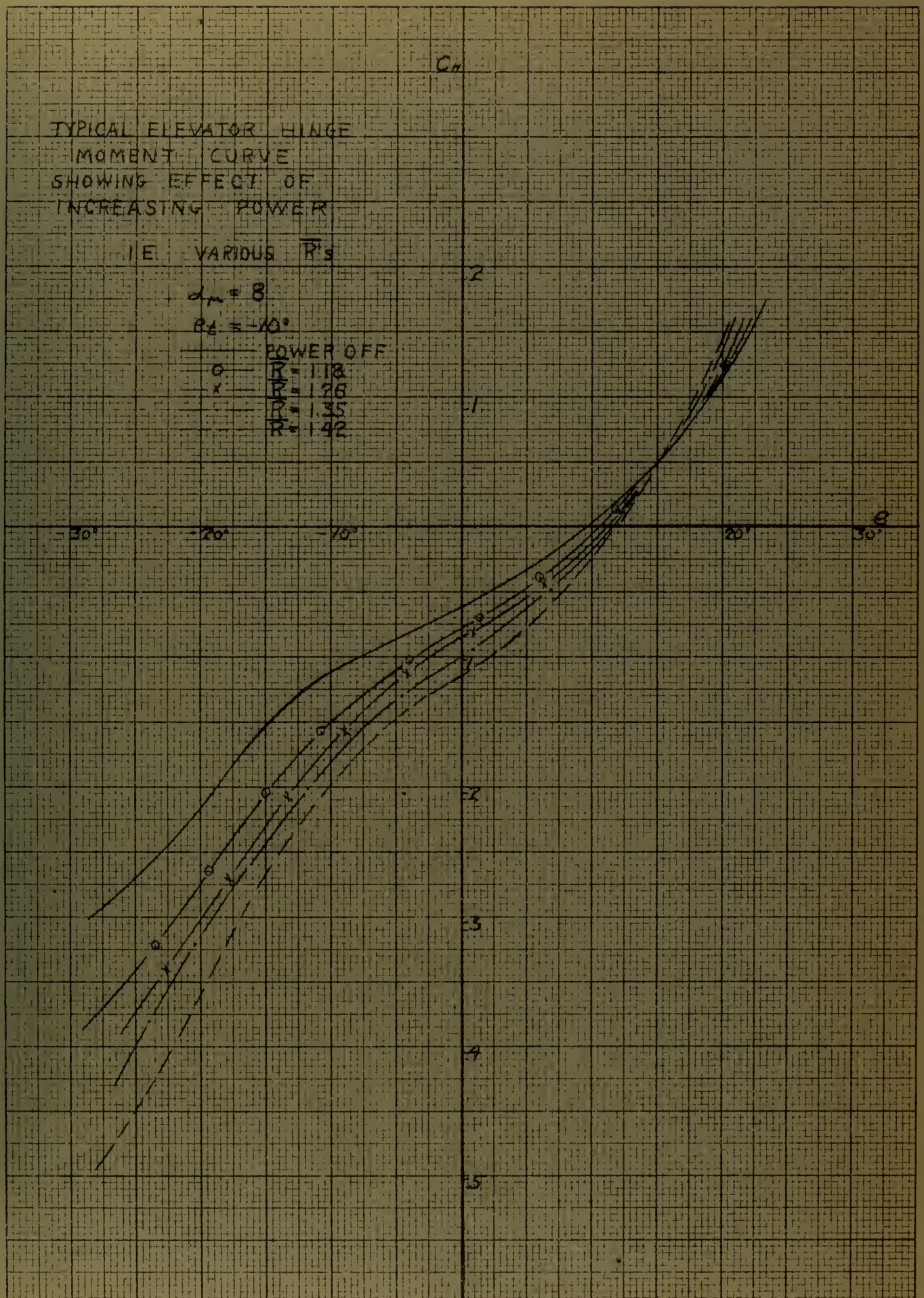
TYPICAL ELEVATOR HINGE MOMENT CURVE SHOWING EFFECT OF INCREASING POWER
IE VARIOUS R's
$\alpha_m = 8$
$\delta_t = -10°$
POWER OFF
R = 1.18
R = 1.26
R = 1.35
R = 1.42
C_H
δ
-30°
-20°
-10°
20°
30°
2
1
-2
-3
-4
-5

FIG. NO. 8

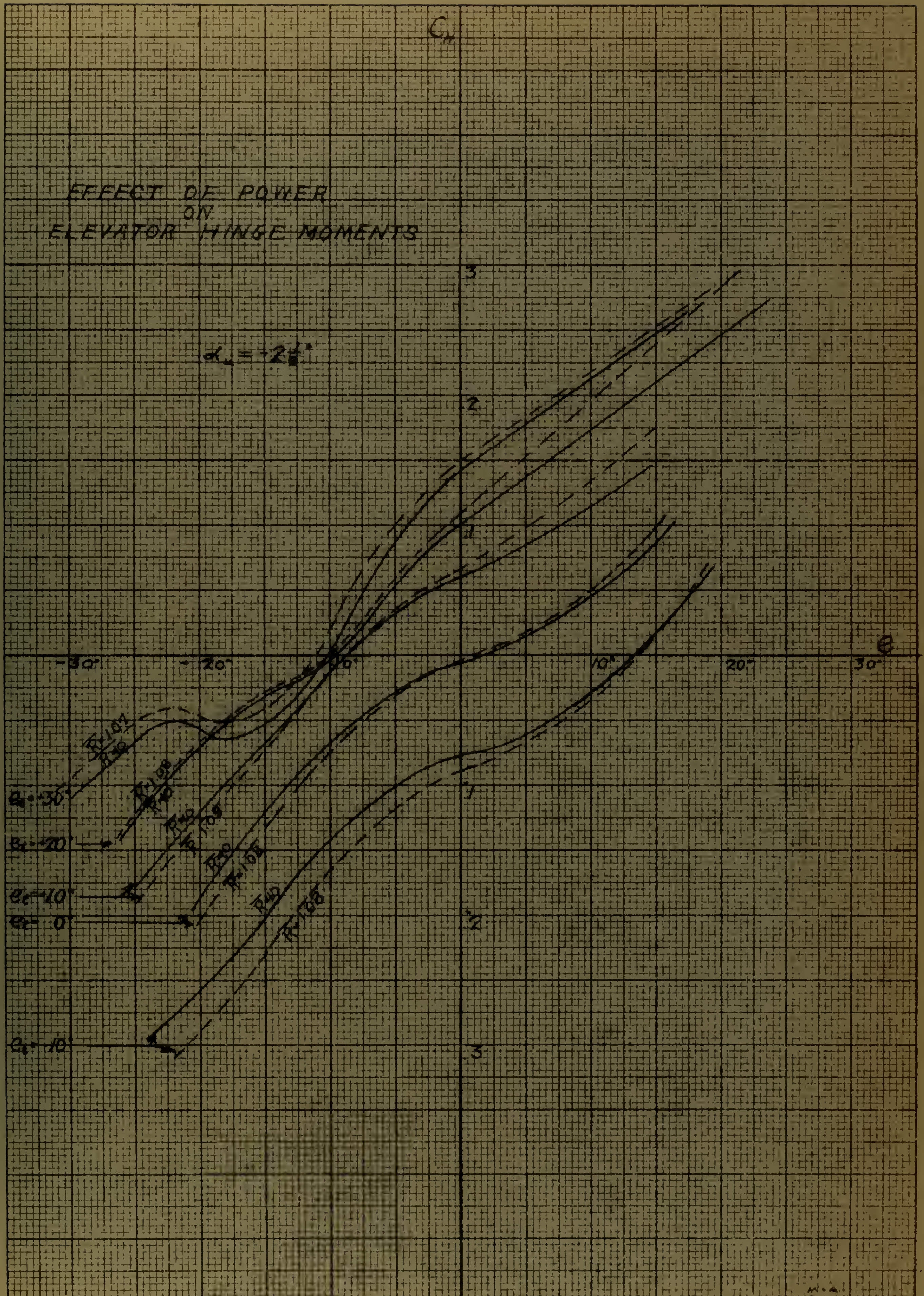
EFFECT OF POWER
ON
ELEVATOR HINGE MOMENTS
C_H
$\alpha_w = -2\frac{1}{2}°$
e
-30°
-20°
10°
20°
30°
3
2
1
.1
.2
.3
$e_t = +30°$
$e_t = +20°$
$e_t = +10°$
$e_t = 0°$
$e_t = -10°$

FIG. NO. 9

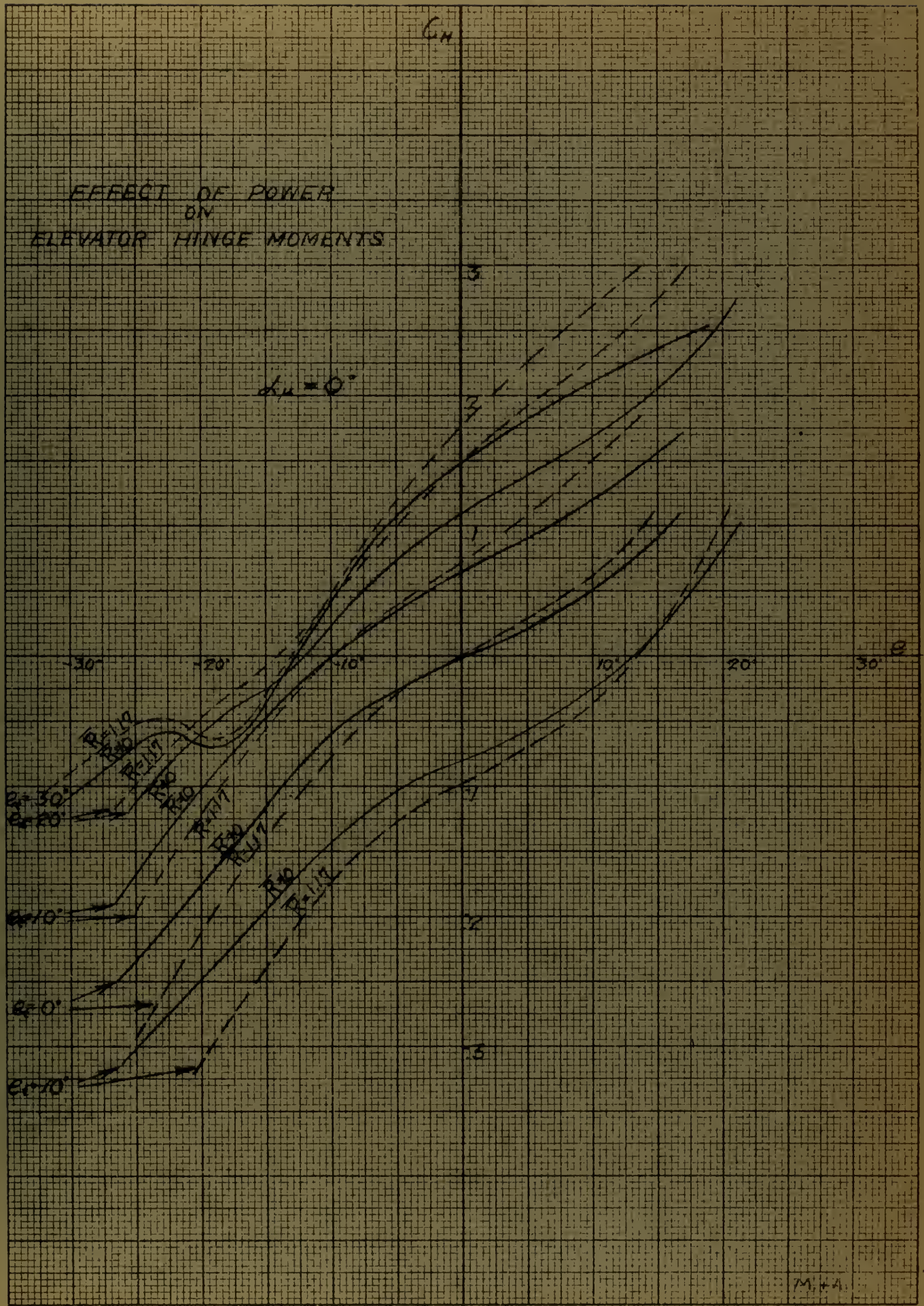
C_H
EFFECT OF POWER ON ELEVATOR HINGE MOMENTS
$\alpha_u = 0°$
.3
.2
.1
-30°
-20°
-10°
10°
20°
30°
θ
$\theta_t = 30°$
$\theta_t = 20°$
$\theta_t = 10°$
$\theta_t = 0°$
$\theta_t = -10°$
R=1.12
R=0
R=.17
M.+A.

FIG NO. 10

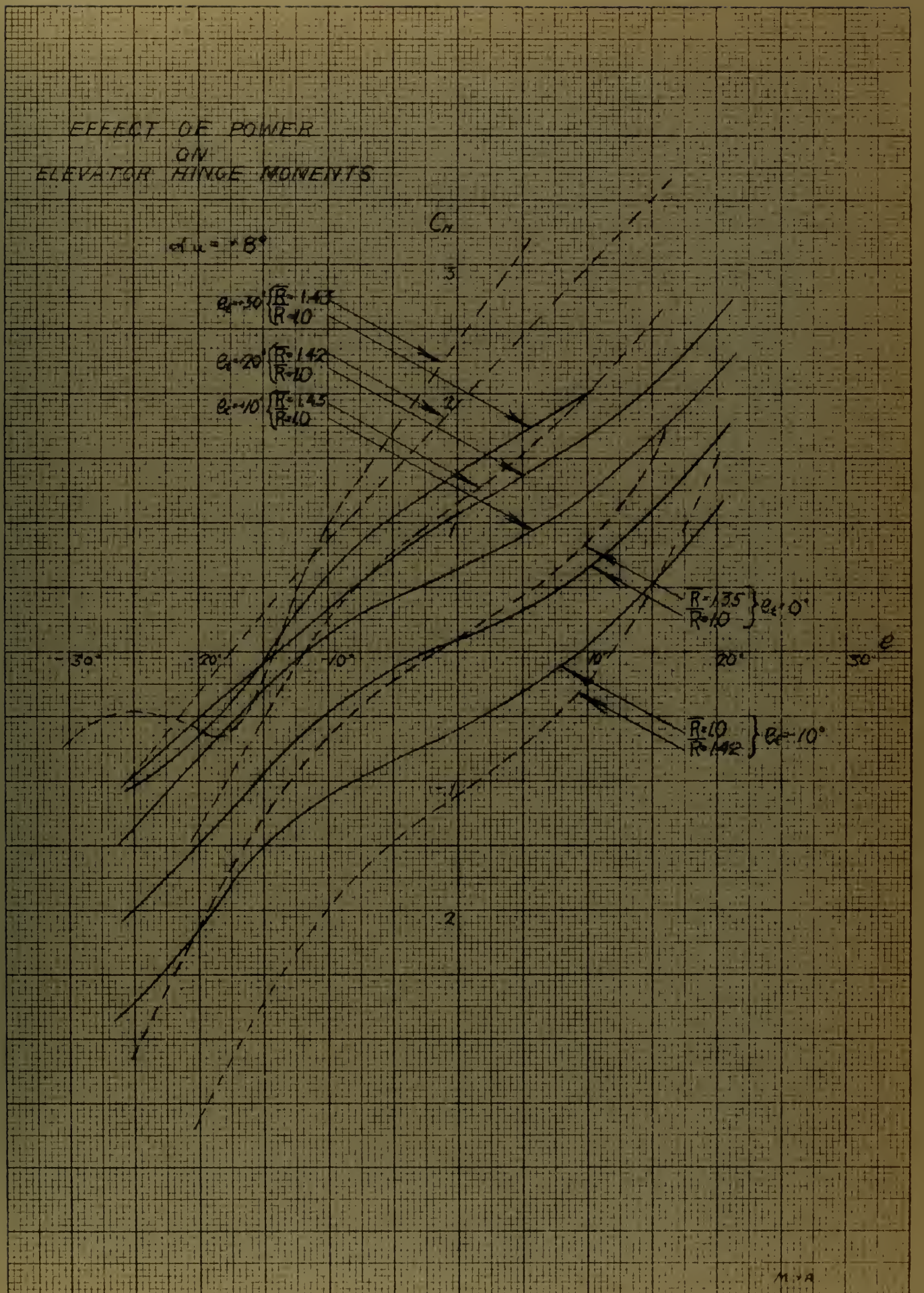
EFFECT OF POWER
ON
ELEVATOR HINGE MOMENTS
C_H
$\alpha_w = -8°$
$\delta_e = -30°$ R=1.43 R=1.0
$\delta_e = -20°$ R=1.42 R=1.0
$\delta_e = -10°$ R=1.43 R=1.0
R=1.35 R=1.0 $\delta_e = 0°$
R=1.0 R=1.42 $\delta_e = 10°$
ϵ
-30°
-20°
-10°
10°
20°
30°
3
2
1
-1
2
M.A.

FIG. NO. 11

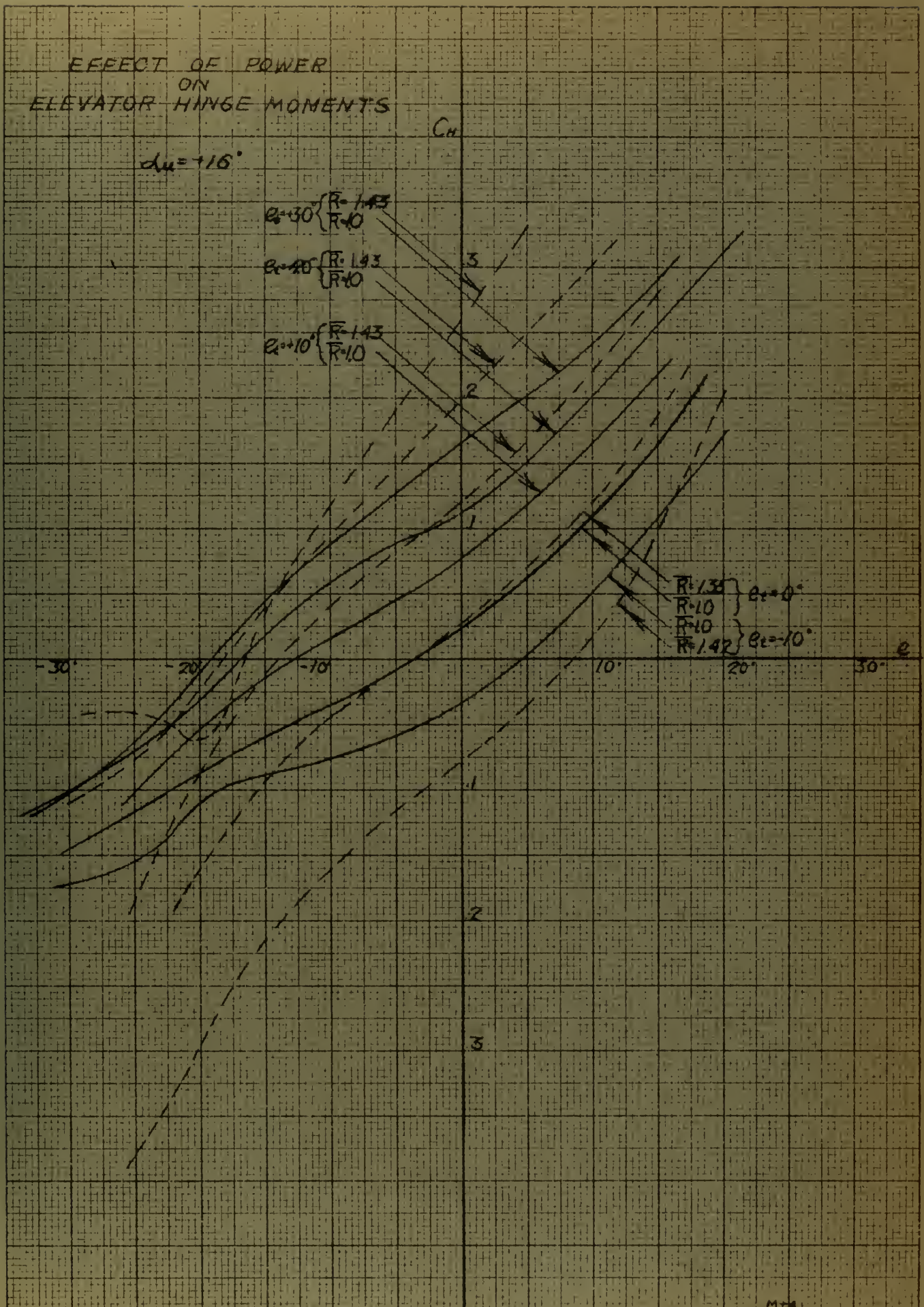
EFFECT OF POWER
ON
ELEVATOR HINGE MOMENTS
C_H
$\alpha_H = +16°$
$\delta_t = +30°$ { R=1.43 / R=1.0
$\delta_t = +20°$ { R=1.43 / R=1.0
$\delta_t = +10°$ { R=1.43 / R=1.0
R=1.33 / R=1.0 } $\delta_t = 0°$
R=1.0 / R=1.42 } $\delta_t = -10°$
δ
-30°
-20°
-10°
10°
20°
30°
3
2
1
.1
2
3

FIG. NO. 12

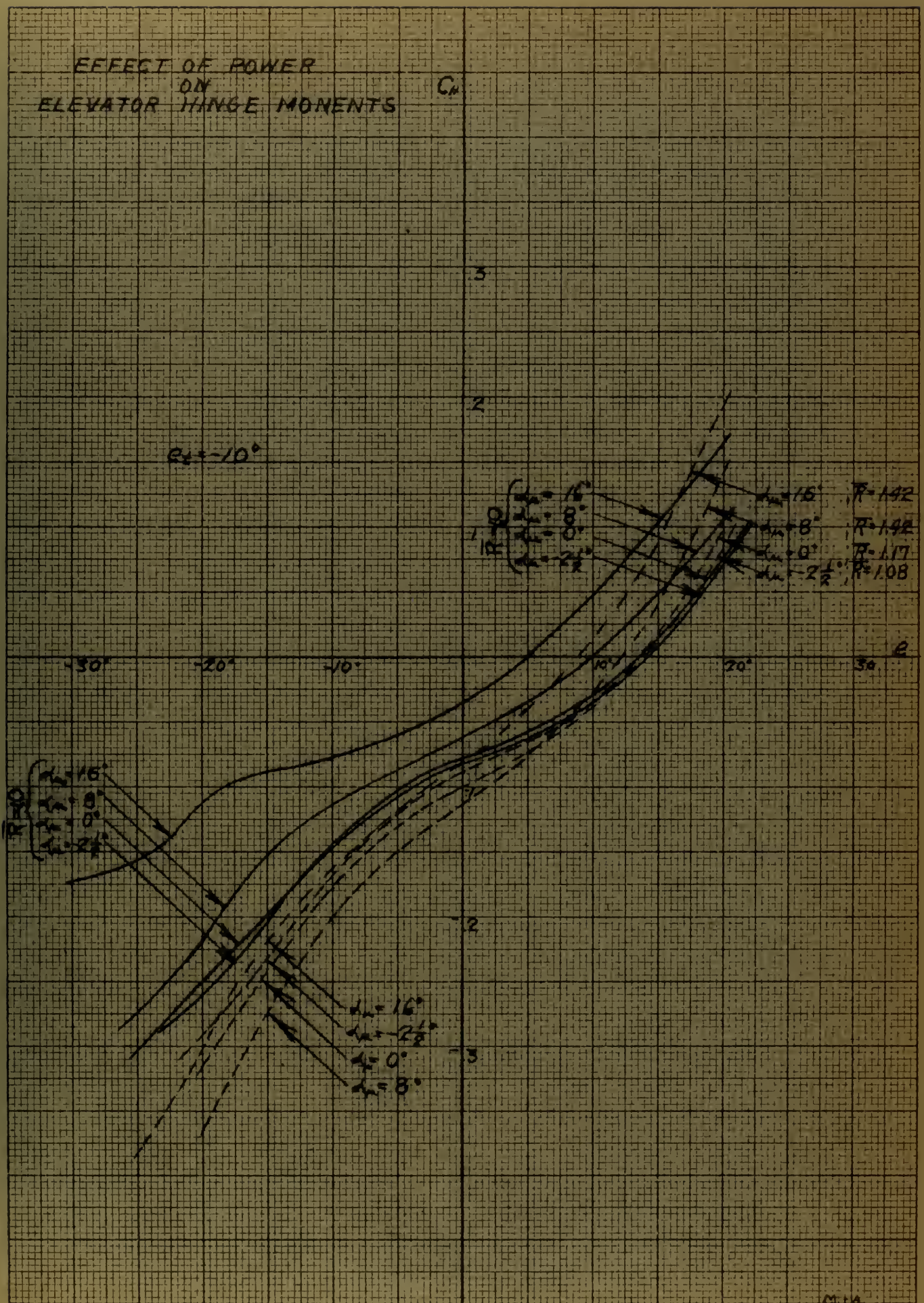
EFFECT OF POWER
ON
ELEVATOR HINGE MOMENTS
C_H
$\delta_E = -10°$
$\alpha_m = 16°$
$\alpha_m = 8°$
$\alpha_m = 0°$
$\alpha_m = -2\frac{1}{2}°$
R = 1.92
R = 1.92
R = 1.17
R = 1.08
-30°
-20°
-10°
10°
20°
30°
δ
3
2
1
-2
-3

FIG. NO. 13

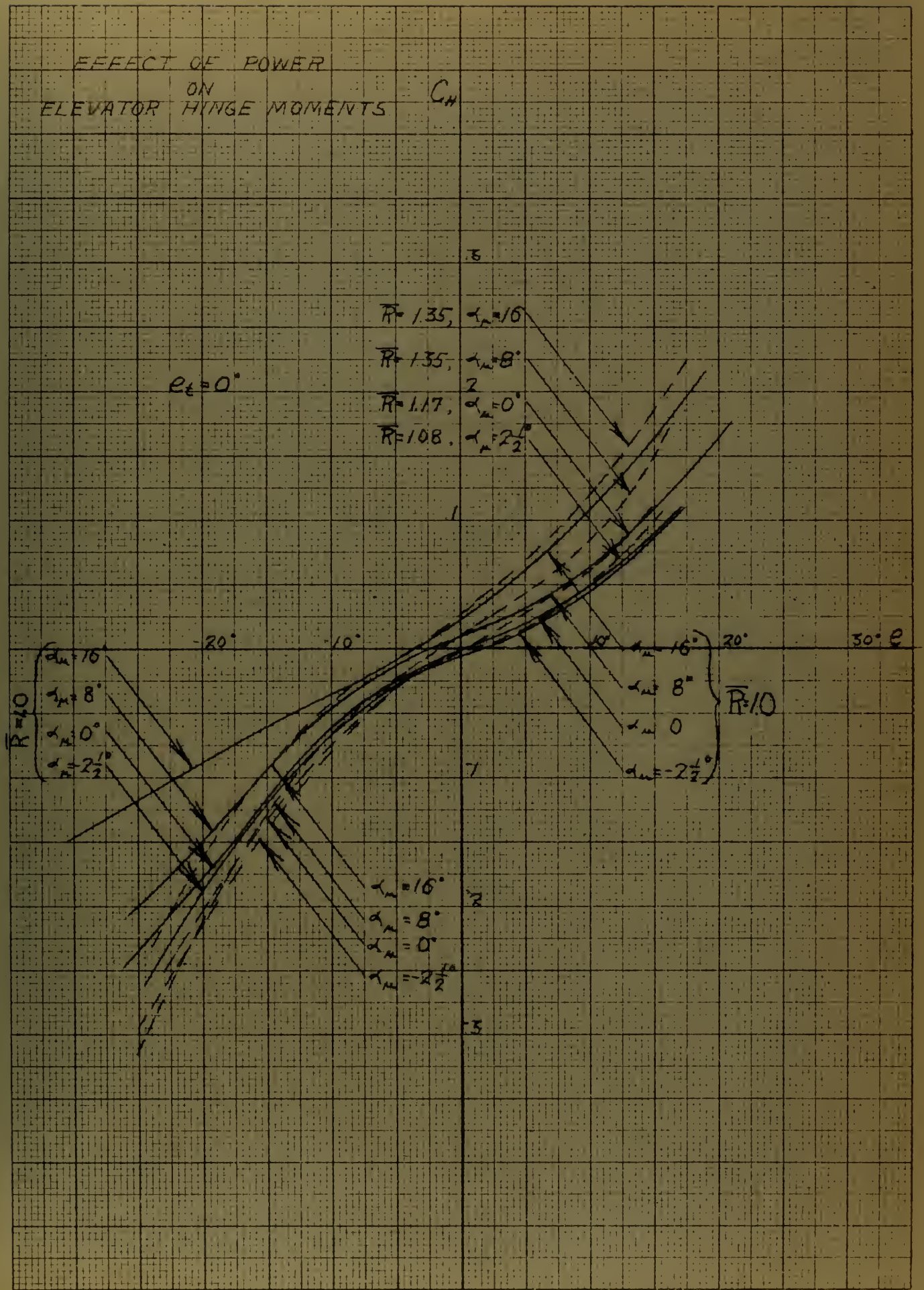
EFFECT OF POWER
ON
ELEVATOR HINGE MOMENTS
C_H
$\bar{R}$= 1.35, α_M=16
$\bar{R}$= 1.35, α_M=8°
$\bar{R}$= 1.17, α_M=0°
$\bar{R}$=1.08, α_M=-2½°
e_t=0°
3
2
1
-1
-2
-3
-20°
-10°
10°
20°
30°
e
α_M=16°
α_M= 8°
α_M 0°
α_M=-2½°
$\bar{R}$=1.0
α_M=16°
α_M= 8°
α_M 0
α_M=-2½°
$\bar{R}$=1.0

FIG. NO. 14

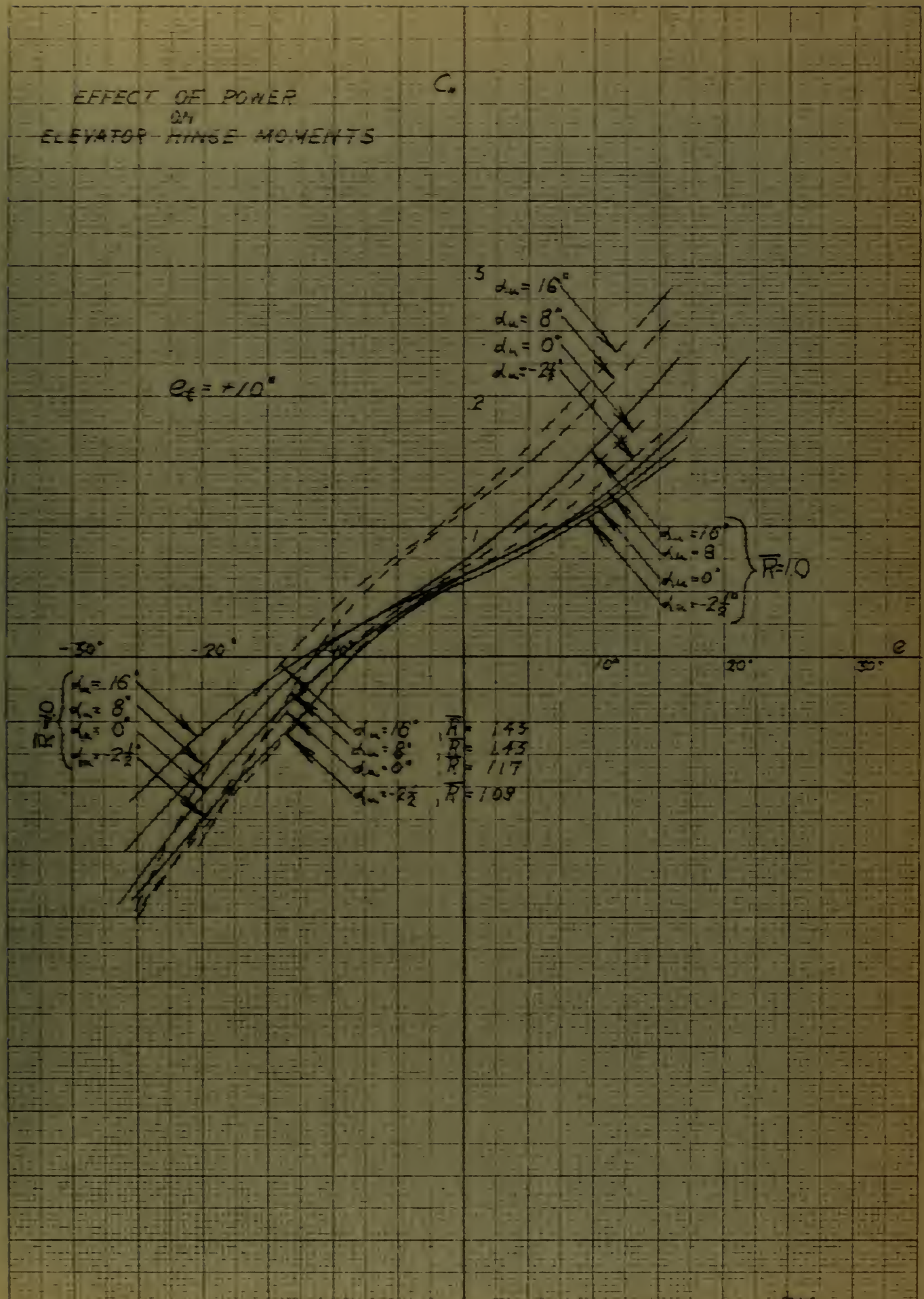
EFFECT OF POWER
ON
ELEVATOR HINGE MOMENTS
C_h
$e_t = +10°$
.3
.2
.1
$\alpha_m = 16°$
$\alpha_m = 8°$
$\alpha_m = 0°$
$\alpha_m = -2\frac{1}{2}°$
$\overline{R} = 1.0$
-30°
-20°
-10°
10°
20°
30°
e
$\overline{R} = 1.0$
$\alpha_m = 16°$
$\alpha_m = 8°$
$\alpha_m = 0°$
$\alpha_m = -2\frac{1}{2}°$
$\alpha_m = 16°$, $\overline{R} = 1.43$
$\alpha_m = 8°$, $\overline{R} = 1.43$
$\alpha_m = 0°$, $\overline{R} = 1.17$
$\alpha_m = -2\frac{1}{2}°$, $\overline{R} = 1.09$

FIG NO. 15

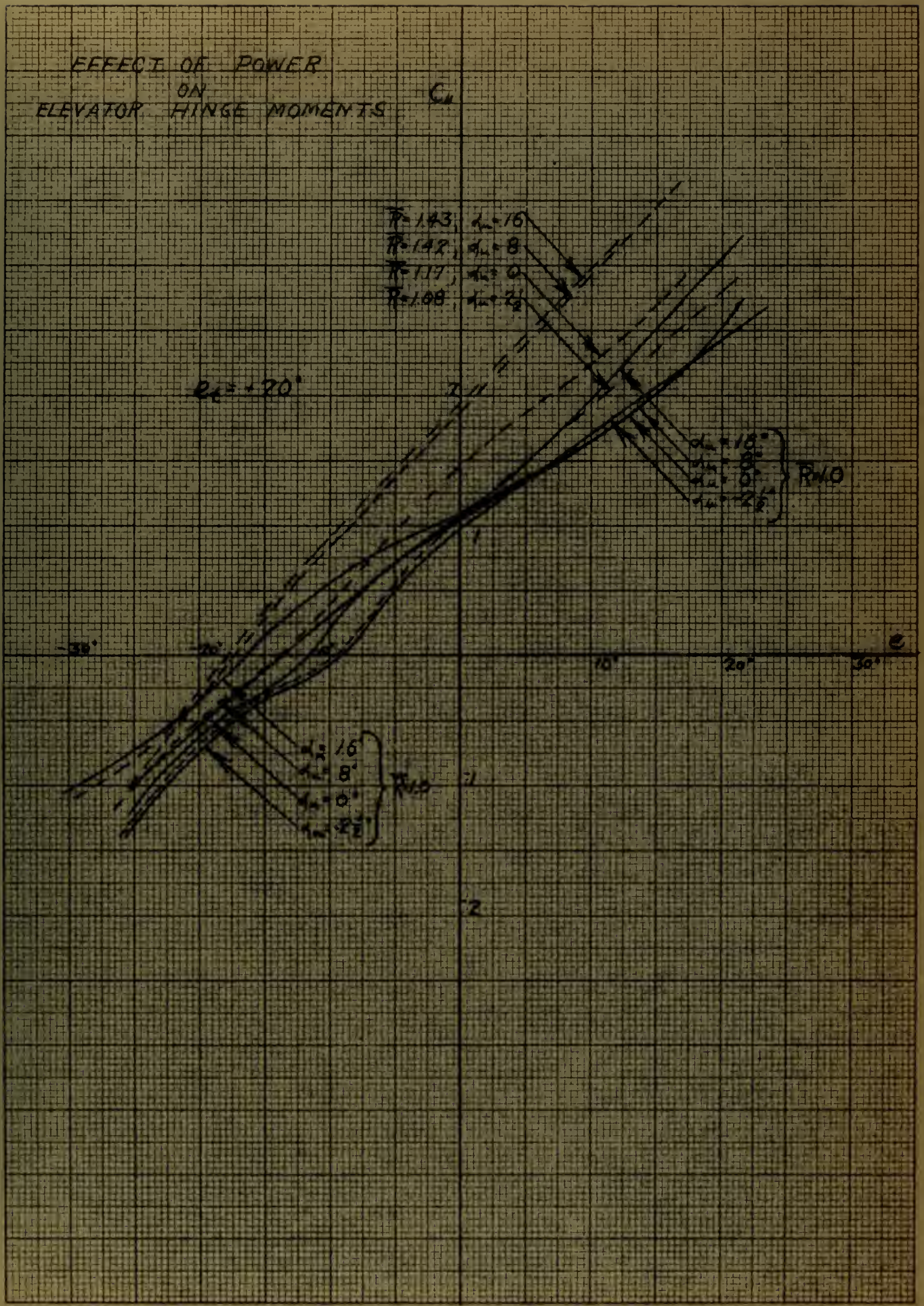
EFFECT OF POWER
ON
ELEVATOR HINGE MOMENTS
C_H
$R = 1.43$; $\alpha_T = 16°$
$R = 1.42$; $\alpha_T = 8°$
$R = 1.17$; $\alpha_T = 0°$
$R = 1.08$; $\alpha_T = -2\frac{1}{2}°$
$\epsilon_t = +20°$
$\alpha_T = 16°$
$\alpha_T = 8°$
$\alpha_T = 0°$
$\alpha_T = -2\frac{1}{2}°$
R=1.0
$\alpha_T = 16°$
$\alpha_T = 8°$
$\alpha_T = 0°$
$\alpha_T = -2\frac{1}{2}°$
R=1.0
-30°
-20°
10°
20°
30°
ϵ
-1
-2

FIG NO. 16

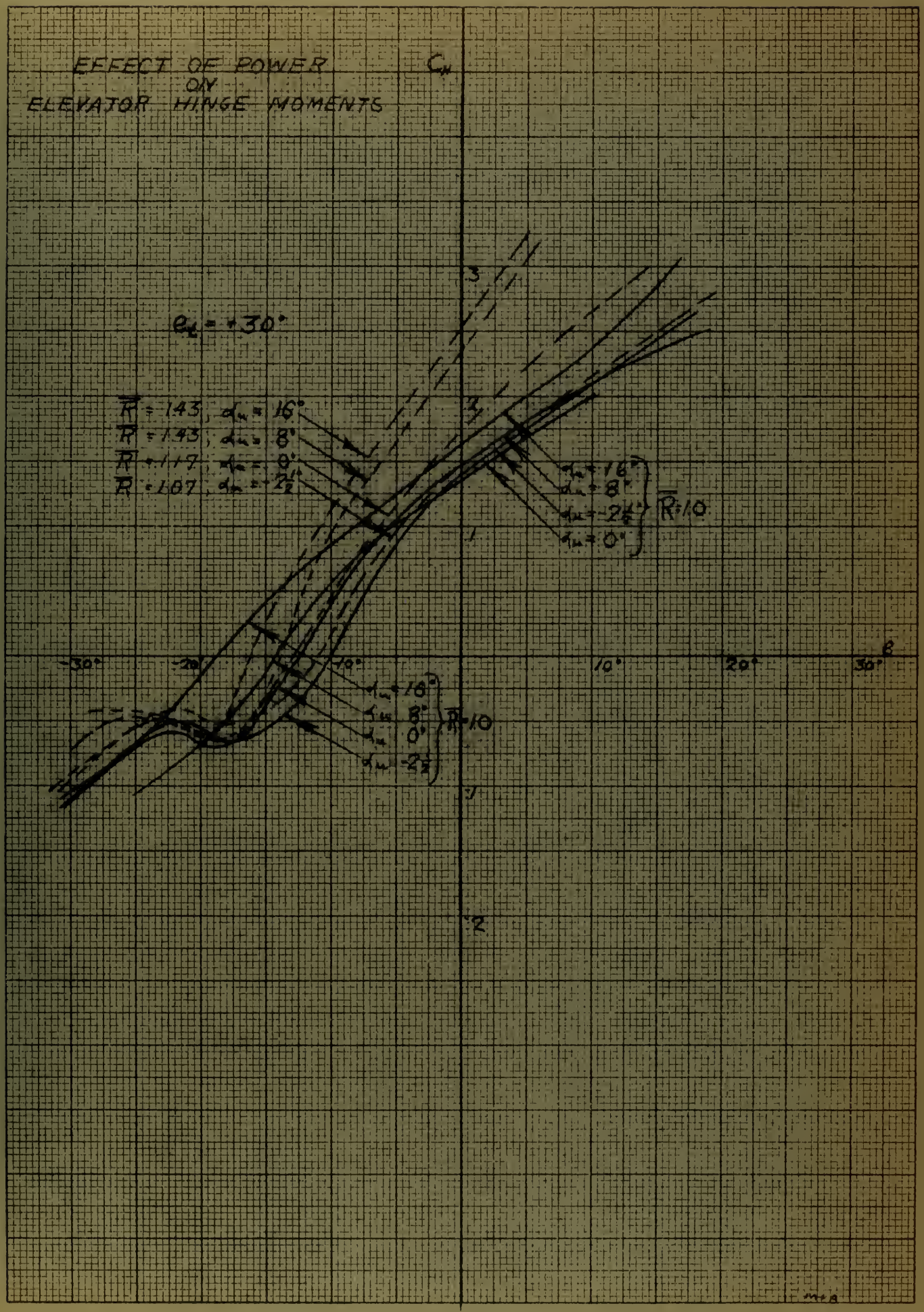
EFFECT OF POWER
ON
ELEVATOR HINGE MOMENTS
C_H
$\theta_t = +30°$
$\overline{R} = 1.43$; $\alpha_H = 16°$
$\overline{R} = 1.43$; $\alpha_H = 8°$
$\overline{R} = 1.17$; $\alpha_H = 0°$
$\overline{R} = 1.07$; $\alpha_H = -2\frac{1}{2}°$
$\alpha_H = 16°$
$\alpha_H = 8°$
$\alpha_H = -2\frac{1}{2}°$
$\alpha_H = 0°$
$\overline{R} = 1.0$
$\alpha_H = 16°$
$\alpha_H = 8°$
$\alpha_H = 0°$
$\alpha_H = -2\frac{1}{2}°$
$\overline{R} = 1.0$
-30°
-20°
-10°
10°
20°
30°
α
3
2
1
-1
-2

FIG. NO. 17

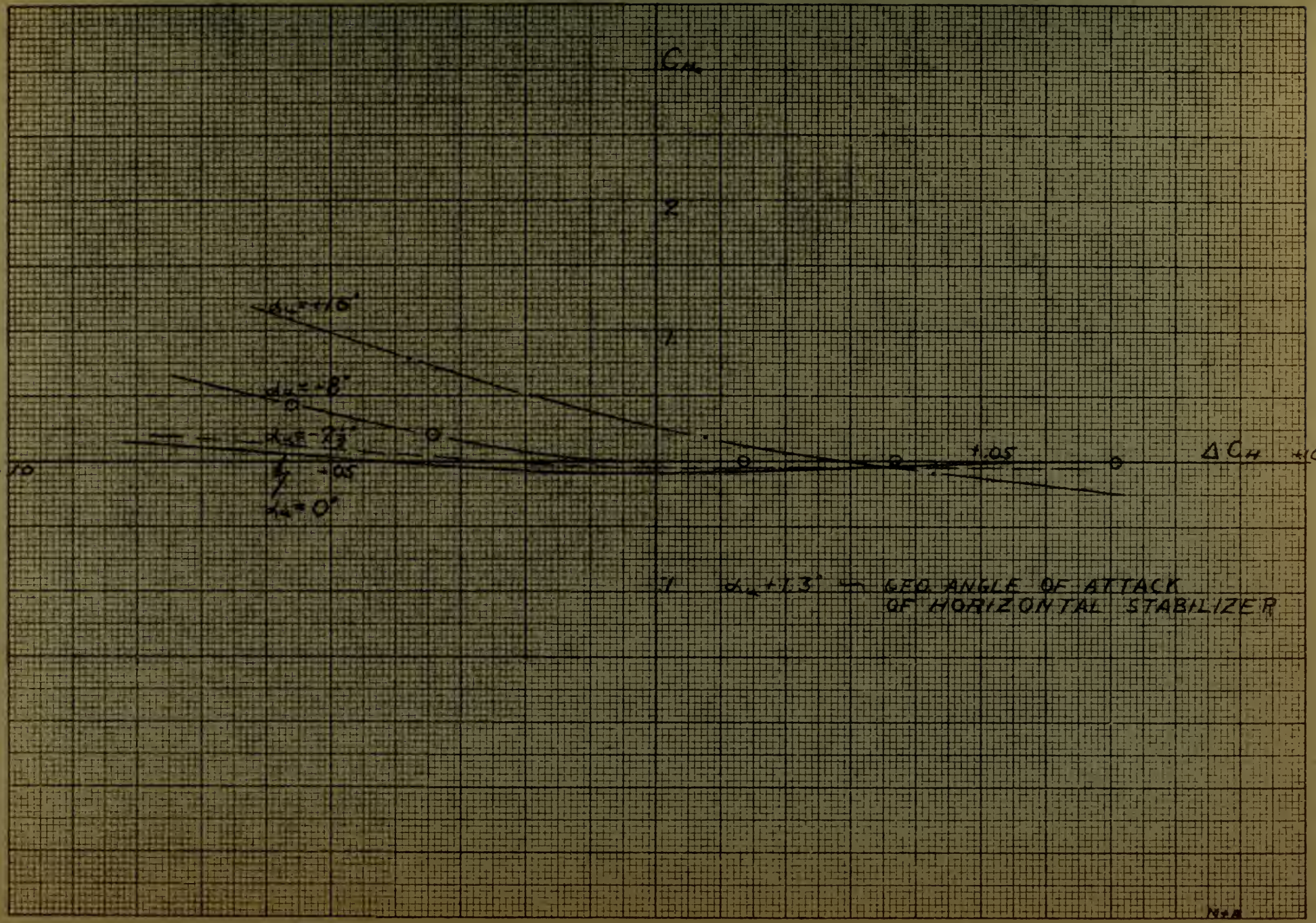
C_H
2
1
$\alpha_t = +1.6°$
$\alpha_t = -8°$
$\alpha_t = -2.4°$
$\alpha_t = 0°$
-.10
-.05
1.05
ΔC_H
α_t +1.3° = GEO ANGLE OF ATTACK OF HORIZONTAL STABILIZER

FIG NO 18

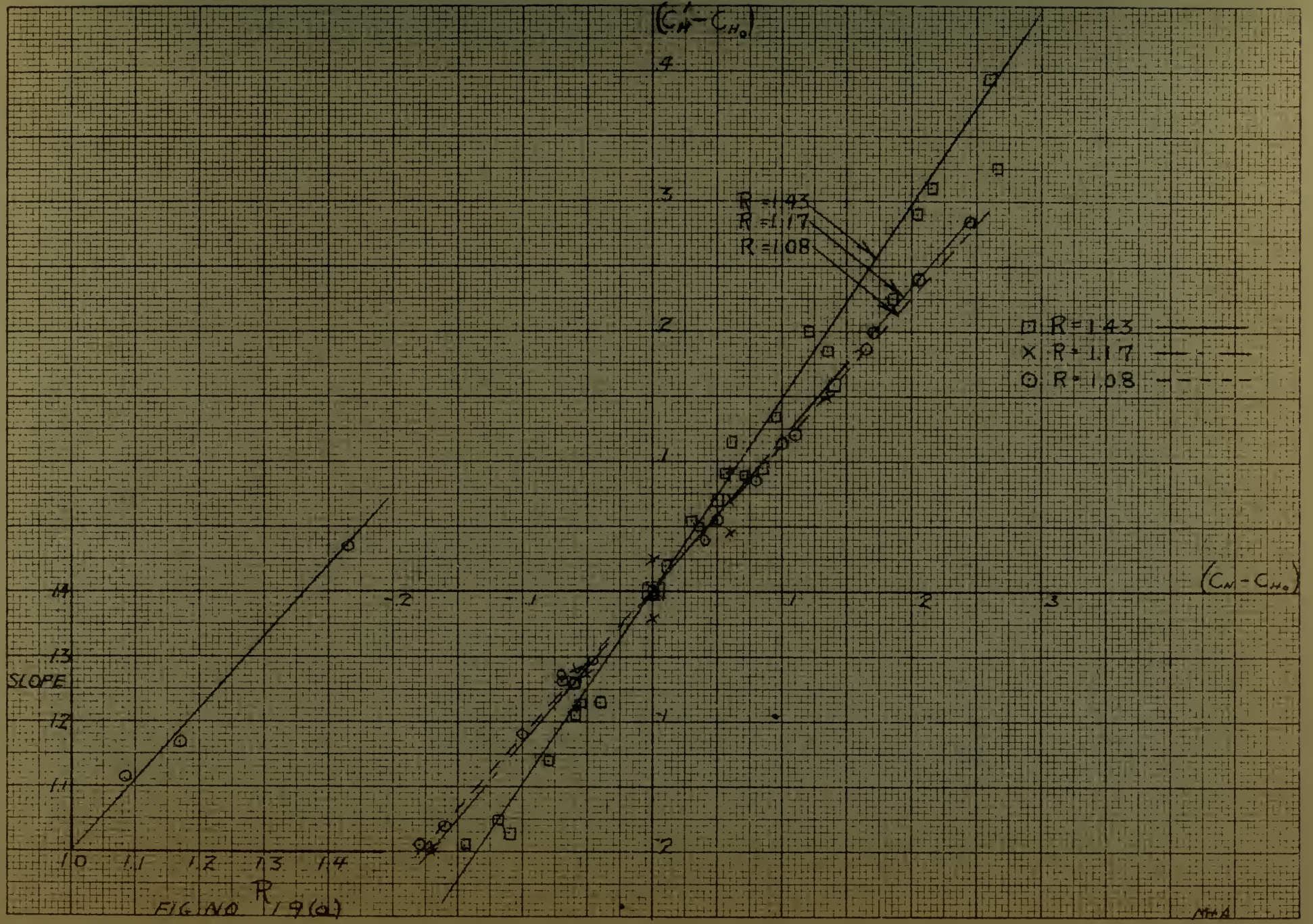

FIG NO 19

3) Plot $\frac{(C_H' - C_{H_o})}{(C_H - C_{H_o})} = f(\overline{R})$ vs. $\overline{R}$ (Fig. 19a)

4) It appears that $\frac{f(\overline{R})}{\overline{R}} = \frac{1.4}{1.36}$. Therefore $f(\overline{R}) \doteq 1.03\ \overline{R}$, or within our experimental limits of accuracy, $f(\overline{R}) = \overline{R}$.

This result is interesting because we should think that the variation would be proportional to the dynamic pressure or $V^2 \backsim \overline{R}^2$, instead of R.

5) Hence our results are approximately expressed by

$$C_H' - C_{H_o} = \overline{R}(C_H - C_{H_o})$$

6) Values of C_{H_o} are plotted in Fig. 18 as function of ΔC_H for various values of α_s = geometrical angle of attack of horizontal stabilizer.

In order to make use of these data, C_H vs. e curves are obtained from wind tunnel laboratory data for model in question at various values of e_t and α_u, with power zero. (No power plant is assumed to be installed on the model). Desiring to determine the effect of power on the hinge moment coefficient, we proceed as follows:

1) Determine ΔC_H as defined above.
2) Enter Fig. 18 with ΔC_H and α_s in question and obtain C_{H_o}. Locate this on C_H vs. e curve for proper α_u and e_t.
3) Compute $(C_H' - C_{H_o}) = \overline{R}(C_H - C_{H_o})$ for various values of "e" and plot result as shown in Fig. 7.

Effect of Power on Static Directional Stability

The effect of power on static directional stability was investigated for two geometrical angles of attack, that is $\alpha_u = -2^\circ$; and $+8^\circ$. The low angle of attack simulated high speed conditions and the high angle, low-speed conditions. The rudder angles ranged from zero to twenty-five degrees, plus and minus, being varied in increments of five degrees. The angles of yaw investigated ranged through twenty-seven degrees on either side of zero. The power parameter employed in this phase of the investigation was "$\bar{R}$" whose significance has been described.

Fig. 20 shows variation of C_y against ψ for various combinations of rudder angle and power for $\alpha_u = -2^\circ$; $q = 30$ gm./sq.cm. Similarly, Fig. 21 is plotted for $\alpha_u = +8^\circ$; $q = 7$ gm./sq.cm.

An examination of these curves shows that a change in rudder angle does not affect stability but merely varies the C_y intercept at $\psi = 0^\circ$. The effect of power also changes the C_y intercept at $\psi = 0^\circ$, and, in addition, it appears to cause an increase in directional stability. This increase is only slightly apparent in Fig. 20, but in Fig. 21, the effect is most noticeable.

In order to explain this increase in static directional stability, with "power on", we resort to a qualitative, graphical analysis. Referring to sketch 9, the vertical tail surfaces are

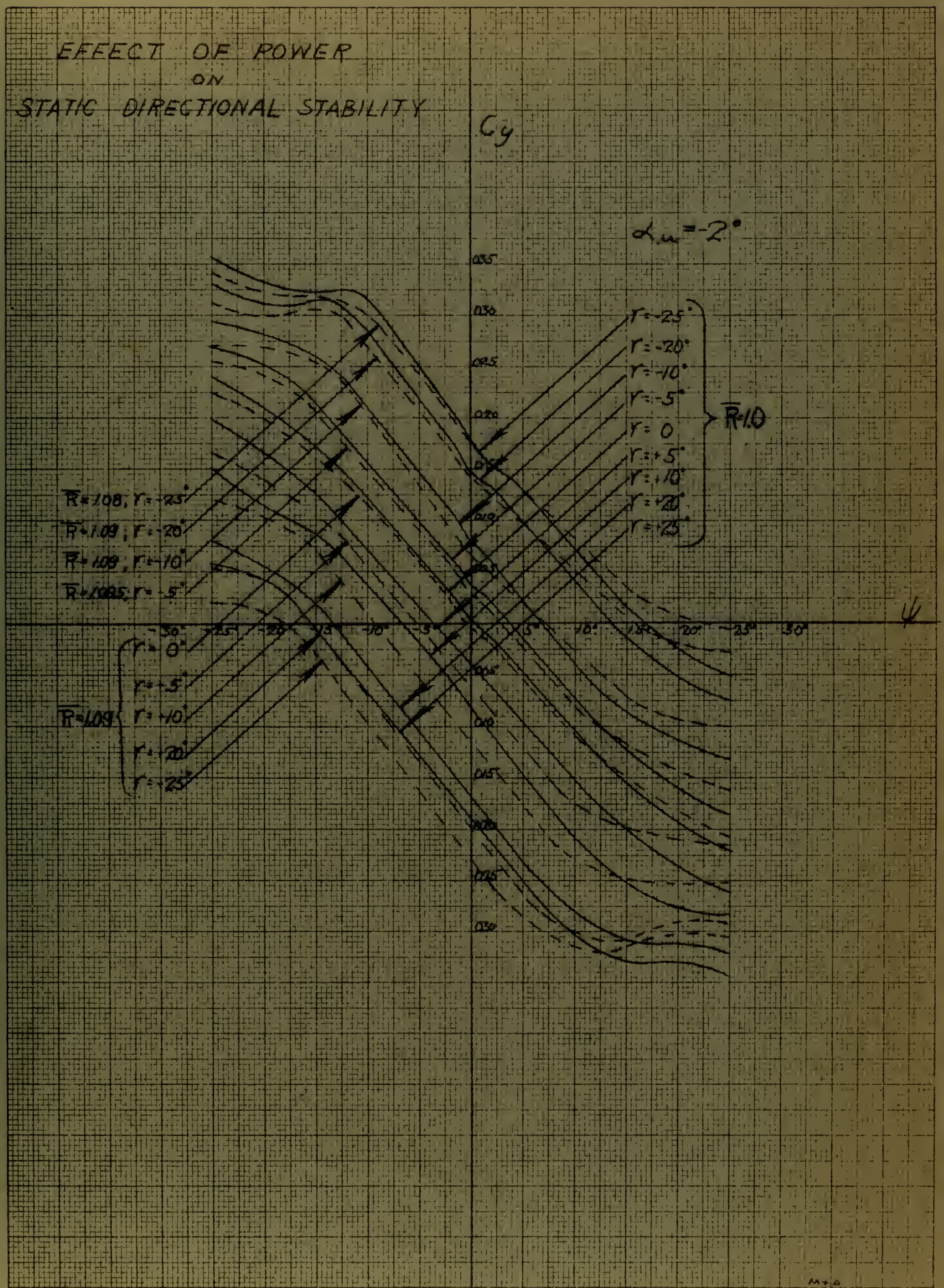
EFFECT OF POWER
ON
STATIC DIRECTIONAL STABILITY
C_y
$\alpha_w = -2°$
.035
.030
.025
.020
.015
.010
.005
.000
.005
.010
.015
.020
.025
.030
$\bar{R}$=1.0
r = -25°
r = -20°
r = -10°
r = -5°
r = 0
r = +5°
r = +10°
r = +20°
r = +25°
$\bar{R}$=1.08, r = -25°
$\bar{R}$=1.09, r = -20°
$\bar{R}$=1.09, r = -10°
$\bar{R}$=1.085, r = -5°
$\bar{R}$=1.09
r = 0°
r = +5°
r = +10°
r = +20°
r = +25°
-30°
-25°
-20°
-15°
-10°
-5°
5°
10°
15°
20°
25°
30°
ψ
M+A

FIG. NO. 20

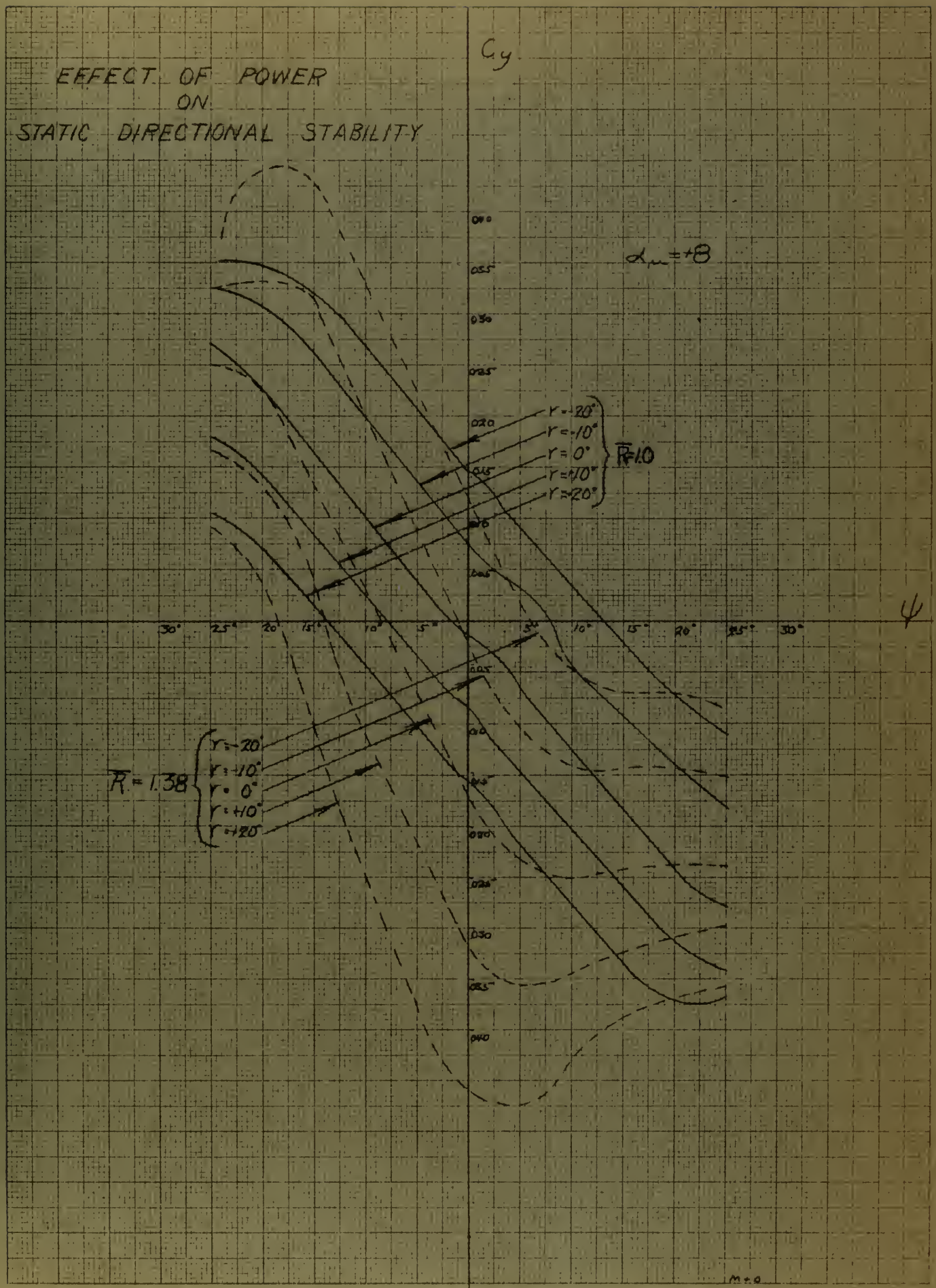
EFFECT OF POWER
ON
STATIC DIRECTIONAL STABILITY
C_y
$\alpha_w = +8$
$\bar{R} = 1.0$
$r = -20°$
$r = -10°$
$r = 0°$
$r = +10°$
$r = +20°$
$\bar{R} = 1.38$
$r = -20°$
$r = +10°$
$r = 0°$
$r = +10°$
$r = +20°$
ψ
30° 25° 20° 15° 10° 5° 5° 10° 15° 20° 25° 30°
M = 0

FIG. NO. 21

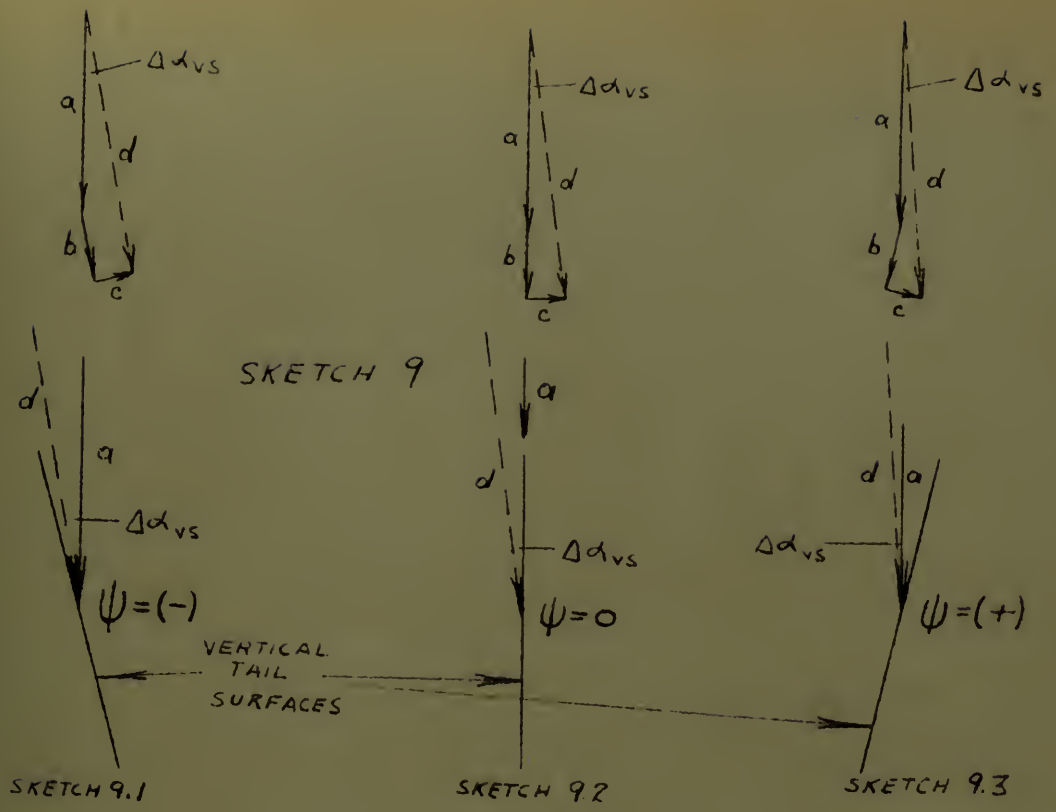
Δα vs
a
d
b
c
SKETCH 9
ψ=(-)
ψ=0
ψ=(+)
VERTICAL TAIL SURFACES
SKETCH 9.1
SKETCH 9.2
SKETCH 9.3

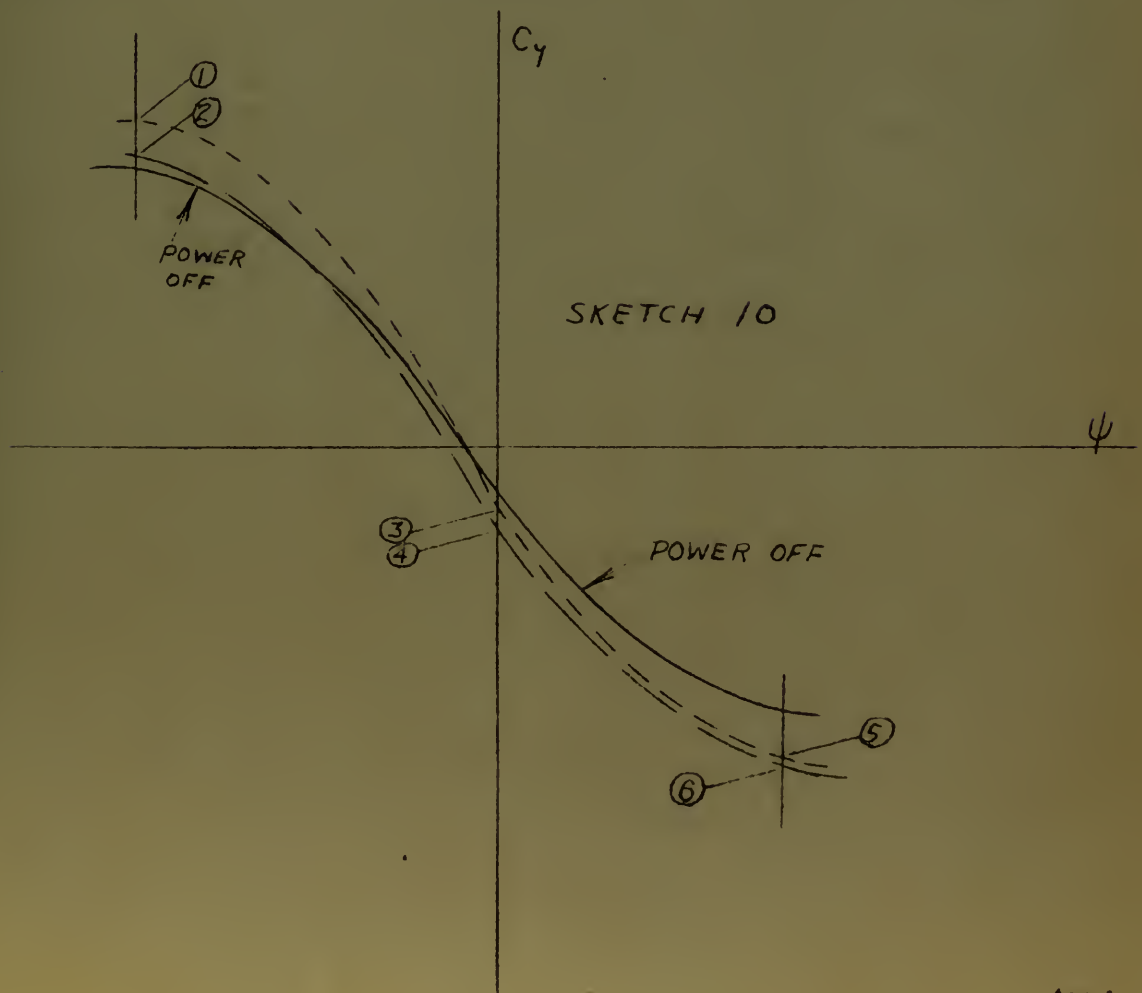
Cy
ψ
POWER OFF
POWER OFF
SKETCH 10
1
2
3
4
5
6

M+A

shown as viewed from above, for the three conditions of negative, zero, and positive yawing angle. Let vector "a" in each case represent the free air flow. Vector "b" in each case represents the slipstream velocity increment parallel to the thrust line. Vector "c", in each case, represents the athwartship component of slipstream velocity due to the upper portion of the slipstream's helix. (The lower portion of the helix is not considered as no vertical tail surface is present in this region.) The resultant vector "d", shown dotted, represents qualitatively the magnitude and direction of the resulting air flow relative to the tail surface. In order to clarify the discussion, vectors "a" and "d" are also shown immediately adjacent to the tail surfaces. We define the angle $\alpha_{v.s.}$, as the geometrical angle of attack of the vertical surfaces relative to the wind vectors, "a" and "d", in each of the three cases.

A typical C_y vs. ψ curve, "no power", is shown plotted in sketch 10.

Now we consider the effect of the increased velocity on directional stability, due to the presence of the slipstream, disregarding, for the moment, the change in the angle $\alpha_{v.s.}$. From this point of view, the curve represented by the dotted line is obtained, for the effect of the increased velocity is to multiply the value of the power-off yawing moment by an

approximately constant factor.

Now we shall consider the effect of the change in the geometrical angle of attack, $\Delta\ \alpha_{v.s.}$, of the vertical surfaces. (We recall that the dotted curve in sketch 10 corresponds to the effect of increased velocity alone.) In the case of negative yaw, $\alpha_{v.s.}$ is changed by the amount $\Delta\ \alpha_{v.s.}$ through the action of the slipstream, as shown in sketch 9.1. This produces a negative change in yawing moment and moves point (1) down to some such position as point (2) in sketch 10. Similarly, at zero yaw, the angle of attack has been changed by a $\Delta\ \alpha_{v.s.}$, but, as is clear from sketch 9.2, the amount of this change is less than before so that point (3) is moved down to point (4), a smaller distance than before. At positive yaw, the angle of attack has changed only very slightly as a result of which point (5) is moved only a short distance to point (6). The final "power-on" curve is shown by the long dashed line.

It is seen that the deviation of this "power-on" curve from the "power-off" curve is quite similar to that of the corresponding experimental curves in Fig. 21. Thus the increase of static directional stability, due to the presence of power, is qualitatively explained.*

---

*In the near future, tests are to be conducted at the GALCIT wind tunnel, with the power model less its tail surfaces, to determine the effect of power on static directional stability due to vertical tail surfaces alone. When these results become available, it is believed that the analysis of this effect of power can be explained on a quantitative basis.

To show the effect of power on static longitudinal stability, we define

$$B = \frac{\frac{dC_y}{d\psi}'}{\frac{dC_y}{d\psi}}$$

where $\frac{dC_y}{d\psi}'$ = slope of C_y vs. ψ curve, power on.

$\frac{dC_y}{d\psi}$ = slope of C_y vs. ψ curve, power off.

Fig. 22 shows a plot of B vs. the power parameter "$\bar{R}$" for the two angles of attack investigated.

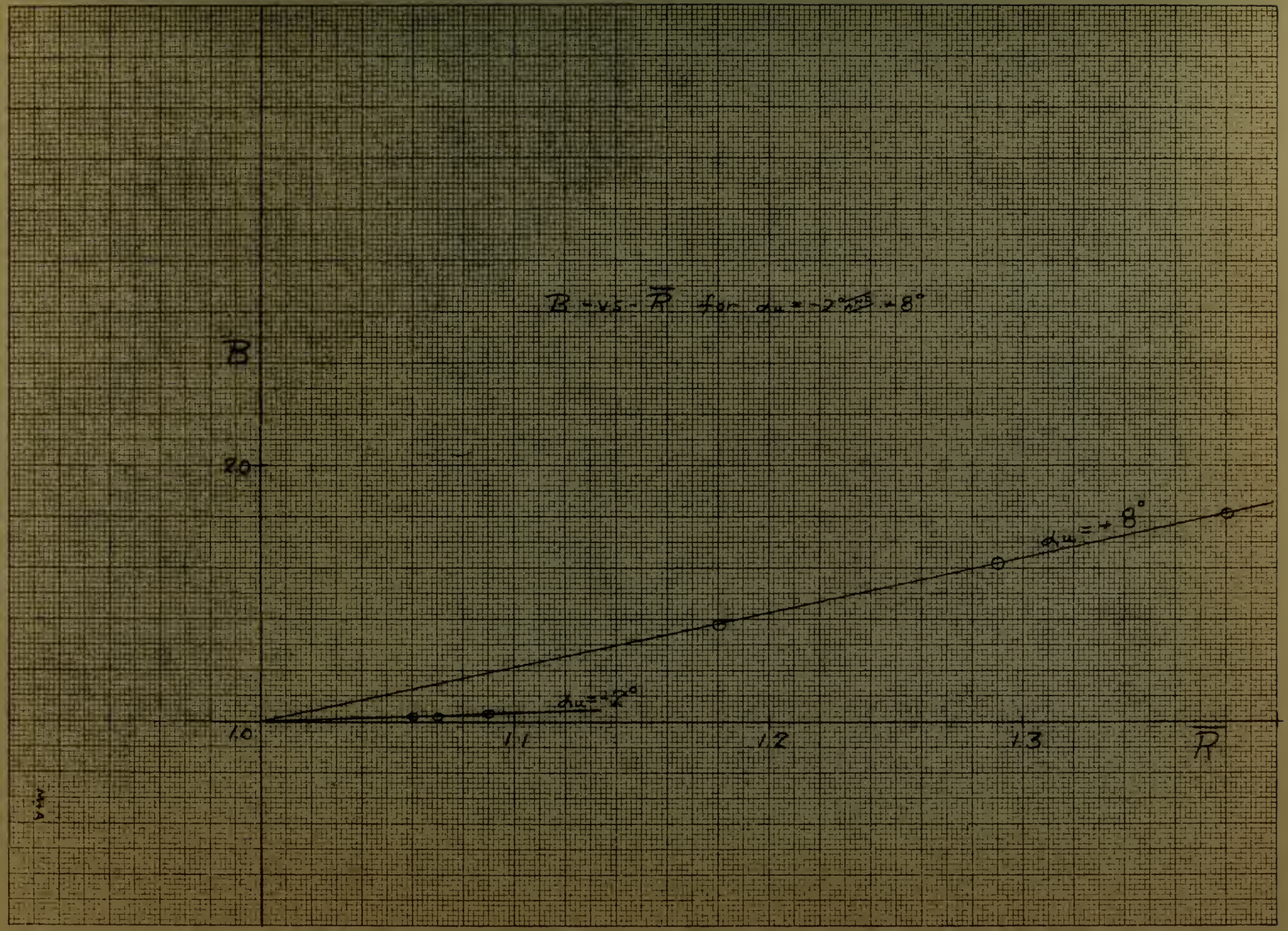
$\bar{B}$ -vs- $\bar{R}$ for $\alpha_w = -2°$ & $+8°$
$\bar{B}$
2.0
1.0
1.1
1.2
1.3
$\bar{R}$
$\alpha_w = +8°$
$\alpha_w = -2°$

FIG. NO. 22

Acknowledgment

The power plant model adds an additional parameter to the difficulty of compiling wind tunnel laboratory data. Without the helpful cooperation of the entire wind tunnel staff, the task of obtaining and compiling the data which have been presented in this paper, would have been well nigh impossible in the time available. The authors wish to express their appreciation at this time to the wind tunnel staff for the gracious assistance rendered. Especial thanks are due Lt.-Comdr. Calvin M. Bolster, U.S. Navy, for curves and data from his Master's Thesis which are included in this report. The authors are deeply indebted to Dr. Theodor von Karman for the inspiration gained through their professional association with him. To Dr. C. B. Millikan, the authors are particularly indebted for his general supervision of the entire project, his keen interest and many helpful suggestions.

Thesis 13678
M59 Miller
c.1 Wind tunnel tests on a low-wing monoplane with propeller running.